



Research article

Parametric study of an empty diffuser geometric parameters and shape for a wind turbine using CFD analysis

Debela Alema Teklemariyam^{a,*}, Eshetu Tadesse Yimer^a, Venkata Rammaya Ancha^b, Balewgize Amare Zeru^a

^a Jimma Institute of Technology, Thermal Energy Systems, P.O.Box 378, Jimma, Ethiopia

^b Jimma Institute of Technology, Sustainable Energy Engineering, Jimma, Ethiopia

ARTICLE INFO

Keywords:

Wind energy
HAWT (horizontal axis wind turbine)
DAWT
Flanged diffuser
Parametric study
CFD

ABSTRACT

This research examines the optimal 3D geometric parameters and shape of empty diffusers to enhance the mass flow rate of the HAWT rotor plane using a detailed parametric study. Previous works have investigated the use of diffusers to augment turbine power output; however, different curvature surfaces and the effects of all associated angles have not been considered for a thorough evaluation. This work mainly focuses on analyzing the effect of opening angles (2° to 22°), inlet shroud angles (8° to 24°), flange height ratios, flange angles (0° and 15°), and shape of the diffuser as well as flanges on velocity, pressure at the diffuser entry, and through the diffuser section at a wind speed of 4.5 m/s. At an inlet-shroud angle of 24° and an opening angle of 8° , with a diffuser flange height-throat diameter ratio of 0.3, the system achieved an 82.9% increase in flowrate. The diffuser with an inlet shroud-side lower stepped flange showed an optimum velocity of 9.12 m/s (maximum) and 8.2 m/s (average), resulting in a 102.66% and 82.2% increase in velocity, respectively. The percentage increase in velocity of the present study is 92.61%, compared with the previous maximum increase in rate of 53.8%, and then an increase in velocity of 38.81% was obtained. The optimum speed occurred at 0.175 m from the inlet section of the diffuser, indicating where the turbine should best be located. The CFD results from this work were validated with experimental data from the literature, showing a good agreement between the two. Integrated diffuser-turbine system simulation and experimental work with field tests are recommended as a way forward.

1. Introduction

Recently, the development and application of renewable energy sources have become more critical issues in many developed and developing countries because of the severe impacts of global warming and the rapid use of fossil fuels. Energy demand keeps rising as these countries attempt to enhance the living conditions of their citizens. The challenge with renewable energy lies in its high initial investment cost and, thus, a higher energy cost. However, developing and developed countries face the issue of lowering energy costs by optimizing existing energy resources.

The world has immense potential for using renewable energy to minimize reliance on traditional fuel sources and increase the electrification rate. One of the most environmentally friendly renewable energy resources is wind energy. Between 2019 and 2021, a

* Corresponding author.

E-mail address: debela.teklemariam@ju.edu.et (D.A. Teklemariyam).

Abbreviation and nomenclature

CFD	Computational fluid dynamics
EES	Engineering Equation solver
SST K- ω	Shear stress transport K-omega model
γ	Inlet shroud Angle
DAWT	Diffuser-augmented wind turbine
\emptyset	The opening angle of the diffuser
θ	Flange Angle
D_t or D_1 or D	The diameter of the throat or inlet diameter of the diffuser
L_D or L	Length of diffuser
Y	Length along y-axis
X	Length along x-axis
3D	Three dimensional
HAWT	Horizontal axis wind turbine
Re	Reynolds Number
H	Height of flange
C_p	Pressure coefficient
DE	Differential Evolution
SSWT	Savonius-style wind turbine
$\frac{U}{U_m}$	Non-dimensional velocity or velocity ratio
<i>Greek symbols</i>	
ρ	Density
μ	Viscosity
γ	Gamma

net capacity of 50–110 Giga-watt wind power was added [1]. A wind power capacity of 93.1 GW was installed by 2021, increasing employment opportunities [2,3]. As a means of advancement, Diffuser-augmented wind turbines (DAWTs) have been extensively studied for quite some time. The oncoming wind is channeled by DAWTs, which creates high velocity around the inlet of the diffuser. The diffuser has drawn much attention [4,5] since it can lead to power augmentation, allowing turbines to operate in places with low wind speeds. In addition, it is used to reduce tip losses and noise and improve safety. Much research shows a significant power increment in DAWT compared to bare wind turbines [6–9]. The performance of unducted and ducted wind/water turbines was discussed using an analytical model [6], and it was concluded that maximum power was obtained for ducted turbines rather than wind turbines without ducts [6,7]. Using neuro-fuzzy estimation, Nikoli [8] also studied diffuser effects on wind turbine performance. The study shows placing wind turbines inside a diffuser can accelerate the wind speed and produce better performance over the bare one with larger power output even at low wind speed. Similarly, the Bontempo and Manna [5] study shows that DAWT produces greater power than a wind turbine alone for the same frontal area. Moreover, the tip clearance assumption resulted in a negligible effect. All these studies indicate that more effort in the optimization of a diffuser is needed to get even greater power.

Moreover, using axial momentum theory and a semi-analytical approach, Bontempo and Manna [10] investigated how duct thrust affected DAWT performance. Both methods show increments in performance compared to bare wind turbines. The semi-analytical approach analyzed the flow features through the DAWT. The study shows the increment of thrust inside the diffuser increases the performance of wind turbines as such.

Performance investigation of a three-bladed vertical-axis wind turbine was discussed using an artificial neural network [11], resulting in an option to find performance [12]. Work shows the velocimetry image of flow on curved DAWT, and the significant use of a low-speed diffuser is shown. Further [13], DAWT flow analyses were analyzed by using the k-epsilon turbulence model, and the work

Table 1

Variables, shapes, and sizes of diffuser models.

Models	Inlet Diameter , Diffuser length and Flange angle	Opening angle (\emptyset) From (2° to 22°).	Flange height (H) (0.1D to 0.8D).	Inlet shroud angle (8° to 24°)	Diffuser shape	Flange shape
A	Constant or They have No Flange Angle and are fixed with models A, C, E, G, H, and I.	Studied	-	-	Fixed	-
B		Fixed	Studied	-	Fixed	Fixed
C		Fixed	-	Studied	Fixed	-
D		Fixed	Fixed	Studied	Fixed	Fixed
E		Fixed	-	-	Studied	-
F		Fixed	Fixed	Fixed	Fixed	Studied
G		Studied	-	-	Studied	-
H		Studied	-	-	Studied	-
I		Fixed	-	-	Studied	-

verifies that diffuser optimization can accelerate the power output of wind turbine.

Furthermore, using Open FOAM, Khamlaj and Rumpfkeil [14] investigated wind turbine performance optimization by considering power, thrust, blade pitch angle, chord distribution, and drag coefficient parameters. Increasing the diffuser's length and nozzle increases the power output; however, the cost also increases. Generally, optimizing the diffuser's shape and blade shows many power increments. A review by Bontempo and Manna [4] assesses the effects of simplification techniques and optimization methods for determining the most feasible power coefficient. The evaluation points out flaws, gaps, and unresolved problems, opening the door for further study and model enhancements. The INVELOX and bare wind turbines were compared, indicating higher power increment for the INVELOX than a bare wind turbine [8,9].

Specifically, for the diffuser-augmented wind turbine [15], the optimum size and shape of the diffuser were not adequately investigated and identified. In a 2D CFD study [16] with the length of the diffuser ($(\frac{L}{D} = 0.1 \text{ to } 2)$) and flange height ($(\frac{H}{D} = 0 \text{ to } 0.2)$), it has been shown that using a diffuser increased wind turbine efficiency, enhanced velocity ratio of 1.5, and more than twice the power potential. The possibility of growing a diffuser-augmented horizontal turbine is shown, and the result is improved. Further work is recommended in the study of [17].

The Trapezium-shaped diffuser is seen to have the most effective wind-gathering effect [15]. Ahmad et al. [18] observed that proper optimization of accelerating devices, including nozzle and diffuser, was needed to boost power output for a wind turbine in a horizontal and vertical orientation. In addition, the DE method was used to optimize the Savonius Style Wind Turbine (SSWT) with semicircular blades in terms of its overall dimensions (turbine height, aspect ratio, and chord length) [19,20].

Three different wind turbine configurations were compared: flange-shrouded wind turbines, shrouded turbines without flange, and bare wind turbines. Velocity and pressure contours are also compared for the three cases. The shrouded or diffuser with flange produced the most power output among the three configurations and was verified by experimental work [21]. The parametric effect of flange angle on the performance of diffuser-augmented wind turbines was investigated in the range of -25° to $+25^\circ$ (to the vertical axis) using CFD. Superior results are obtained with optimum low pressure at the diffuser outlet and more fluid flow through the diffuser at a 15° flange angle, for reducing cost and producing high power output for the same length and diameter of the diffuser [16,22], and [21]. It is understood that there is much more to be done in future work [16]. However, previous results do not give tangible results about the best possible shape of the diffuser and optimum design parameters like opening angles (2° to 22°), inlet shroud angles (8° to 24°), flange height ratios from ($\frac{H}{D} = 0.1 \text{ to } 0.8$), flange angles (0° and 15°), and shape of diffusers and flanges as indicated in Table 1 of diffusers [15,16,21–24], and all these parameters were studied and analyzed in this work.

Previous works have investigated the use of diffusers to optimize wind speeds; however, different curvature surfaces and the effects of all angles are not considered, which shows the uniqueness of this work.

The dimensions of the upper and lower stepped diffuser models, with 111.2 mm at the inlet and 146.2 mm at the outlet from upstream to downstream of the specific curve, are new parameters.

The effect of side upper-stepped and side lower-stepped profiles over the flat diffuser was investigated. Side upper and lower steps over the diffuser structure with a radius of 0.1D for five curves at equal intervals were investigated.

In the inlet shroud stepped flange diffuser, the lower stepped flange parameters of the radius of curvature ($R_c = \frac{0.1D}{2}$) on the flange section at equal distances were studied rather than making the flange part all section curvature.

Hence, this research deals with optimizing the diffuser size (opening angle, inlet shroud angle, flange height, and flange angle) and shape (forward-upper stepped, forward-lower stepped, side-upper stepped, and side-lower stepped) to maximize the fluid speed, especially for rural electrification applications employing small wind turbines that can operate at relatively lower velocities. The target is to enhance power output by exploiting the cubic relationship with wind velocity. Therefore, diffuser design, parametric study, and shape were investigated in this study. The study covers modeling different shapes and sizes of diffusers in Solid Works and simulation in ANSYS software, accompanied by methodology validation with results reported in the open literature. In addition, the present diffuser is aimed at the horizontal axis of the wind turbine. Even though a system simulation with a diffuser integrated with a horizontal wind turbine is needed, only an empty diffuser is considered here for limited resources. Experimental work and field tests are proposed to be carried out apart from assessing the wind directionality effects on account of the presence of diffusers as future work.

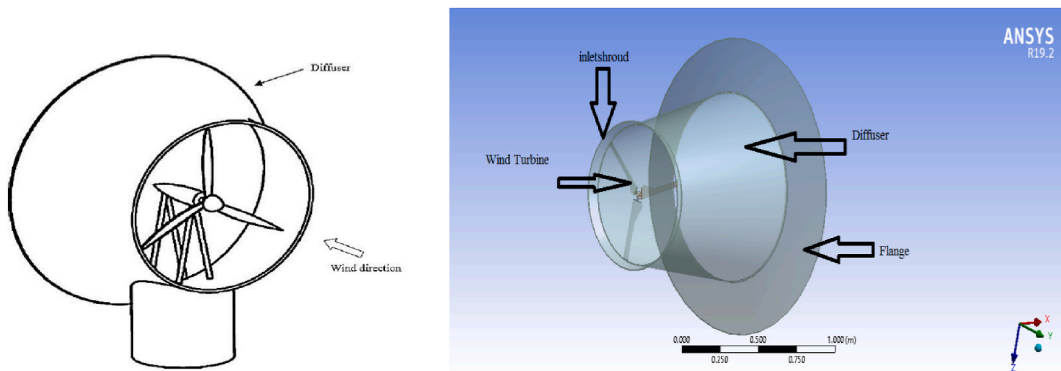


Fig. 1. (DAWT concept) [25] (left) and a general overview of the diffuser with HAWT (right).

However, Fig. 1 illustrates the integration of a diffuser with a horizontal axis wind turbine from the literature (left) and presents a diffuser and a precise suitable dimension of diffuser parametric study, as indicated in Fig. 2, Fig. 4, Fig. 5, Fig. 6, Fig. 7, Fig. 8, Fig. 9, Fig. 10, and Table 1.

2. Materials and methods

2.1. Methodology

Referring to Fig. 2 and using the methods described in Fig. 3, the following design parameters and different diffuser shapes were investigated in this study: In designing and modeling the diffuser, the inlet diameter and length of the diffuser variables are kept constant since they have a cost implication for higher dimensions.

The ratio of diffuser length to the inlet diameter is 1.25, the ratio of flange height to the inlet diameter is 0.5, and the inlet throat diameter or inlet diameter of the diffuser (D) is 0.72 m, as demonstrated in Ref. [26], with a thickness of 5 mm. The other parameters are varied; see Fig. 2.

Diffuser length (L or L_D) is the distance from the diffuser inlet diameter to the diffuser outlet diameter through the central axis, as shown in Fig. 2.

Flange height (H) and shape are part of the diffuser, added at the end of the diffuser exit divergent section to decrease the pressure and increase velocity. The flange shape was not considered in the previous literature. The flange height with minor ratio differences was taken as the significant parameter for diffuser parametric optimizations [16,27,28], and [29].

The flange angle (θ) is the angle from the vertical axis of the diffuser exit end to the left or the right for representing the flange position from the vertical axis, as illustrated in Fig. 2 below. The diffuser flange angle was taken to be 15° as verified by El-Zahaby et al. [22].

Opening angle (\varnothing) The angle from the diffuser's central horizontal axis to the upper or lower wall is included in the investigation to study the effect on the velocity and identify the optimum parameter.

The models considered were explained in detail in the following section, starting from model A, indicated in Figs. 4, Fig. 5, Fig. 6, Figs. 7, Fig. 8, Fig. 9, Fig. 10, and summarized in Table 1.

Model (A): flat diffuser.

It is modeled to study the opening angle (\varnothing) of the diffuser, as shown in Fig. 4 and Table 1.

Model (B): Flanged flat diffuser.

(Diffuser with the addition of flange), and in this case, the flange height (H) was studied. Flange height to throat diameter ratios are investigated in the range of 0.1–0.8, keeping other parameters constant, as shown in Fig. 5 and Table 1, and for the maximum opening angle.

Model (C): Inlet shrouded flat diffuser.

In this part, the effects of the inlet shroud structure were investigated for the angle variation range of 8° – 24° , with 2° angle increments and with the other parameters as constant with the maximum opening angle for 0.1D length of the inlet shroud.

Model (D): Inlet shroud-flanged flat diffuser.

A combination parametric study of (4° to 28° with 4° increments) inlet shroud angle(γ) and constant flange length diffuser structure was investigated to know the combination advantages of inlet shroud and flange.

Model (E and F): forward stepped diffuser (forward upper and lower stepped diffuser).

For the dimensions of the upper stepped and lower stepped diffuser models, the opening angle range of 4° – 20° with 4° increments was investigated with 111.2 mm at the inlet and 146.2 mm at the outlet from upstream to downstream of the specific curve.

Models (G and H): side-stepped diffuser (side upper stepped diffuser and side lower stepped diffuser), respectively.

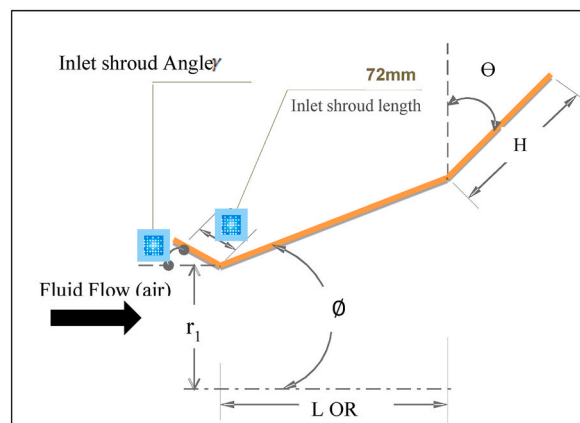


Fig. 2. Axisymmetric geometry represents two-dimensional diffuser parameters.

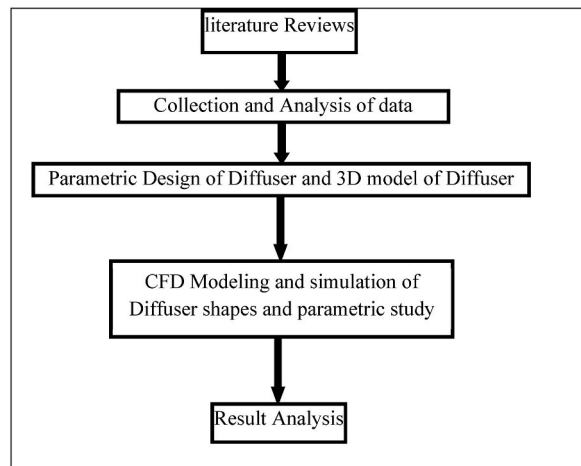


Fig. 3. Studies methodology.

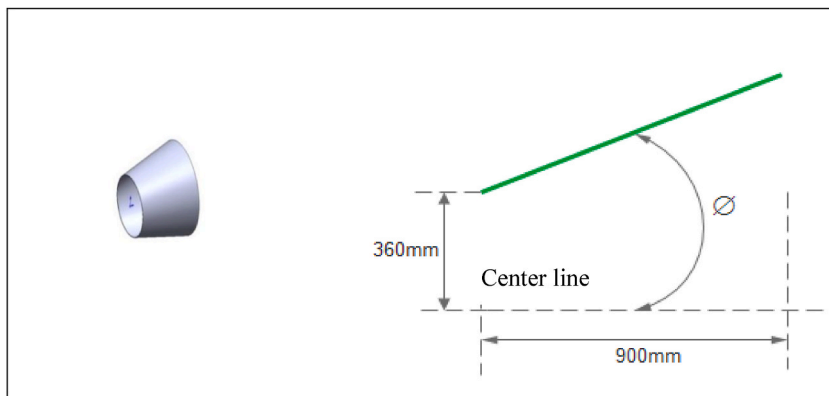


Fig. 4. 3D flat Diffuser model (Left) and 2D flat Diffuser model (Right).

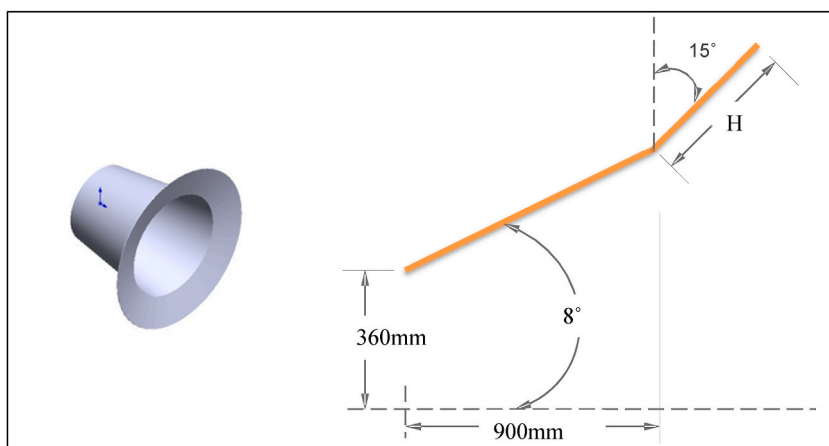


Fig. 5. 3D flanged flat diffuser model (left) and 2D flanged flat diffuser model (right).

This model compares the effect of side upper-stepped and side lower-stepped profiles over the flat diffuser. side upper and lower stepped over the diffuser structure with a radius of 0.1D for five curves at equal intervals were investigated.

Model (I): inlet shroud-lower stepped flange diffuser.

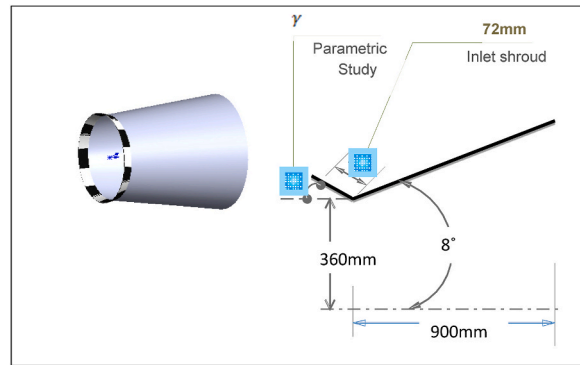


Fig. 6. Inlet shroud flat diffuser (3D left) and inlet shroud flat diffuser (2D right).

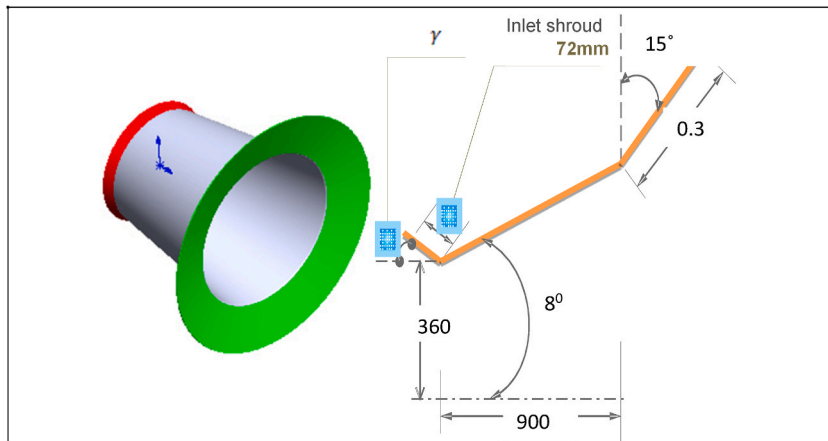


Fig. 7. 3D inlet shroud-flanged flat diffuser (Left) and 2D inlet shroud-flanged flat diffuser (Right).

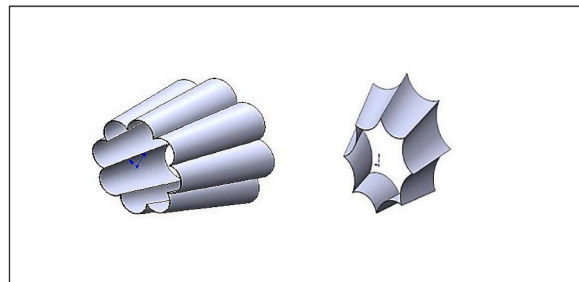


Fig. 8. Forward upper stepped diffuser (Left) and forward lower stepped diffuser (Right) models.

In this case, the lower stepped flange parameters of the radius of curvature ($R_c = \frac{0.1D}{2}$) on the flange section at equal distances were studied.

These models (E, F, G, H, and I) were investigated to see the effect of diffuser and flange surface configurations with a flat surface. The initial idea was to test the designs to comprehend the evolving consequences vis-à-vis the desirable shape; even though, at first instance, they may not look realistic for practical implementation, the results can show the way forward.

2.2. Methods in CFD analysis

Although expensive, exploratory prototyping may not always produce the intended outcomes. CFD simulations are significantly more preferred than experimental prototyping for affecting cost, time, and effort savings through virtual reality testing in different environments, according to Jafari and Kosasis [30]. Given this, the CFD approach is used here.

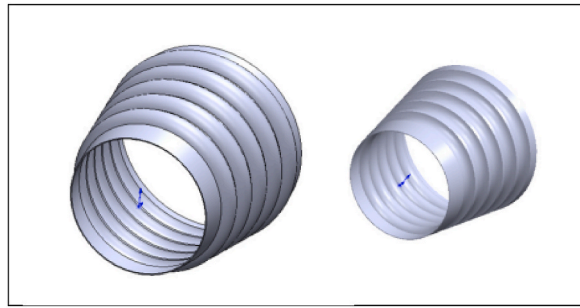


Fig. 9. Side upper stepped diffuser (left) and side lower stepped diffuser (Right).

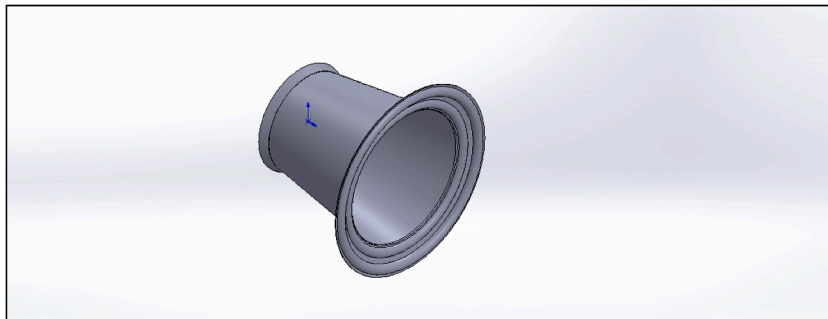


Fig. 10. Inlet shroud-stepped flange diffuser model.

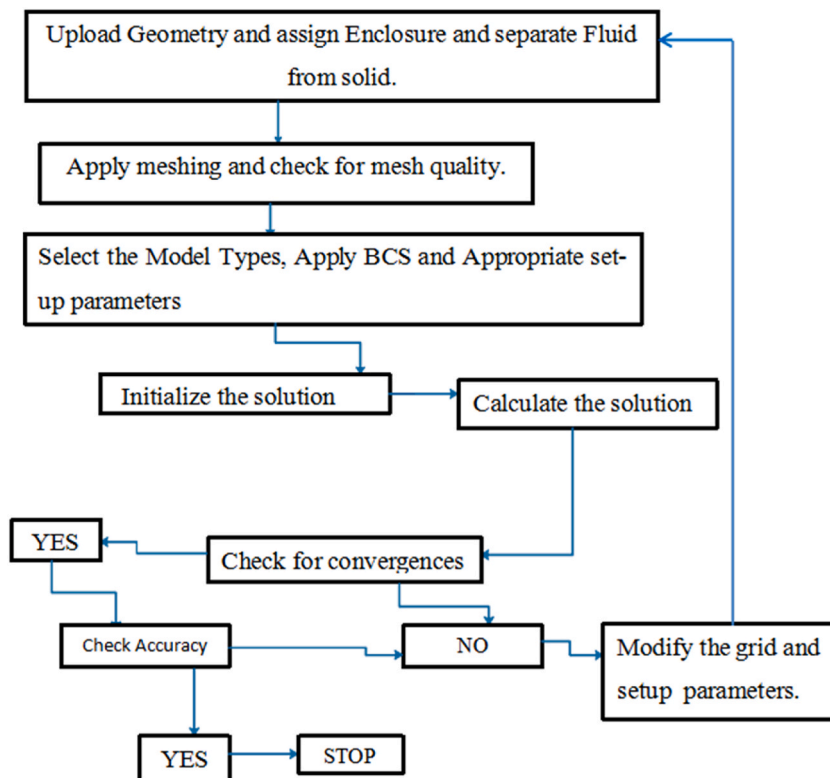


Fig. 11. Flow diagram of computational fluid dynamics analysis procedures for the presented work.

The CFD approach is essential when the flows to be investigated are complex, linear, or non-linear, challenging to solve in experiments because of the material problem, and not possible and tedious to solve analytically. The basic CFD analysis steps are geometry creation, meshing, establishing setup, and applying boundary conditions (see Fig. 11).

2.2.1. Geometry creation

Varied sizes and shapes of diffuser models, as shown in Fig. 12 below, are considered, with descriptions of each parametric size and shape listed in Table 1.

A 3D diffuser was modeled in the SOLIDWORKS package and saved in a Parasolid format for proper ANSYS features and quality of objects.

Jafari and Kosasis [30] used an enclosure with a 4 m diameter and a 10 m length (cylindrical domain) for the simulation of a diffuser with a wind turbine to study the effect of the inlet diameter and size of the diffuser with a rotor radius of 650 mm and a wind speed of 10 m/s. In addition, Al-Quraishi et al. [31] used a 40 cm \times 125 cm enclosure dimension for the diffuser shape with a diameter of 16 cm, a length of 0.5D, and a 0.2D flange length for simulation. In the present work, the simulations were done within an enclosure of a virtual wind tunnel having a diameter of 10 m and a length of 11 m (cylindrical domain). The used chamber was reasonable to control the effect of free-stream turbulence for an inlet diameter of 0.72 m and constant diffuser length compared with the studies mentioned earlier, and no turbulent impact between the wall of the enclosure and the free-stream domain was observed.

After the diffuser was modeled, for each model, the enclosure with a diameter of 10 m and 11 m in length (cylindrical domain), as shown in Fig. 13, was sketched to create the fluid part over the diffuser. The diffuser was placed at the center of the enclosure, 3 m from the inlet section. The chamber on the imported diffuser underwent a Boolean operation, creating the fluid domain areas. The fluid region is obtained by subtracting the diffusers from the enclosure (see Fig. 14).

2.2.2. Meshing

The fluid computational domain was discretized into small elements and nodes to know and study the effects of fluid flow associated with the diffuser kept inside the enclosure for each node after the geometry creation of each model. The model was created in solid work and imported to the ANSYS modeler while differentiating the fluid and solid domains separately in the design modeler.

Since tetrahedral mesh elements could also be precisely adjusted to any geometry and were entirely unstructured, tetrahedral meshing was adopted in this investigation [32]. These element types were used in wind turbines by Parsa and Maftouni [21] and Al-Quraishi et al. [21,31], and [33] to construct a grid of diffusers throughout the enclosure. In addition, face meshing and edge sizing were used, as indicated in Fig. 15.

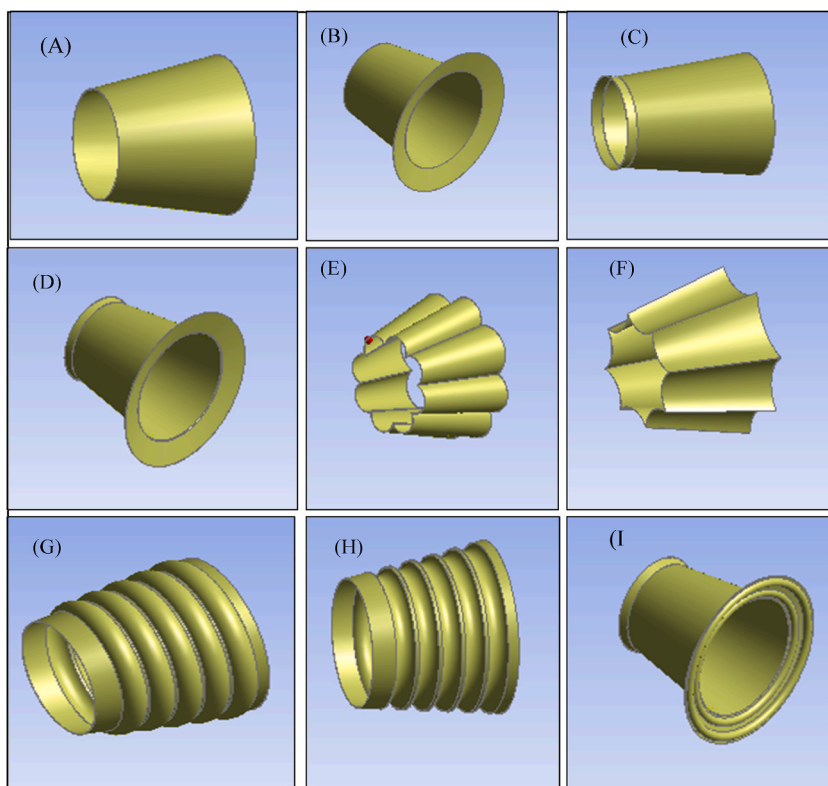


Fig. 12. Diffusing geometry models for the presented work.

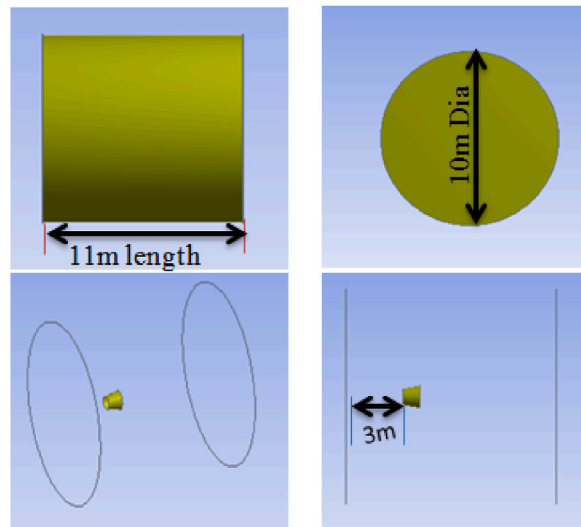


Fig. 13. The diffuser geometry has an enclosure fluid domain.

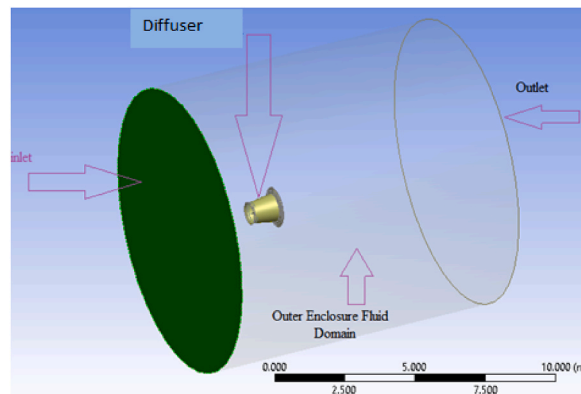


Fig. 14. Diffuser geometry and outer fluid domain.

2.2.3. Fluent setup

2.2.3.1. Operating conditions.

i. General

The steady-state flow simulation was used throughout this work because unsteady flow requires much longer time and computational resources than steady flow, as also employed in other studies [21,30].

Gases can be taken as incompressible flow within 5% of density change, which translates to a Mach number of less than 0.3, or when the velocity of flow is less than 30% of the velocity of the sound [34,35]. Hence, within the Mach number range of $0.013 < 0.3$, the airflow is assumed to be incompressible, and gases at low speeds (such as those applicable to wind velocity ranges) are considered incompressible fluids [36].

Hence, the pressure-based solver is selected to solve the problem of incompressible, subsonic, and low-speed flows.

ii. Models

Selecting the best-performed turbulence model is essential in calculating and extracting superior results in CFD, as discussed in Section 2.3 below.

iii. Materials

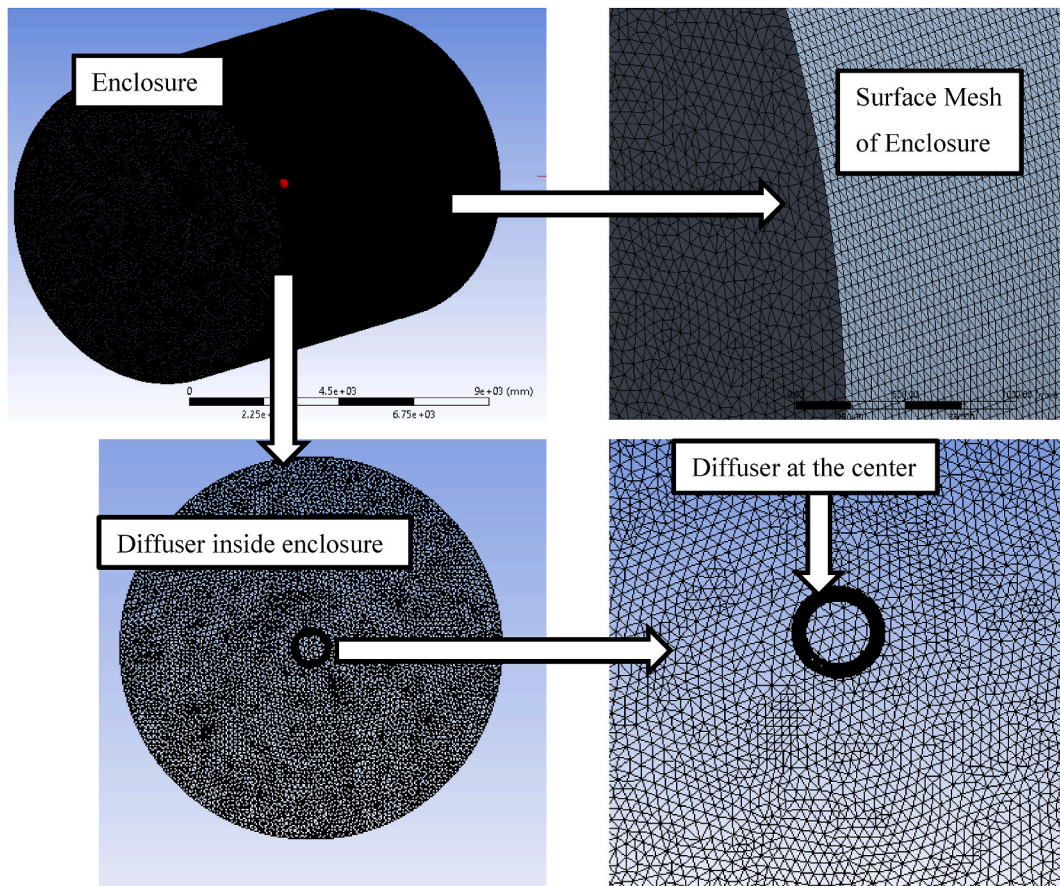


Fig. 15. Mesh features of the enclosure and diffuser.

The materials used for the fluid domain were air, and the materials for the solid diffuser were Aluminum.

2.2.3.2. *Boundary conditions.* For all the walls, a no-slip boundary condition was assumed [21].

Boundary conditions in CFD fluent, specified in Fig. 16 and Table 2, were used in this paper. Flow flows out of the computational domain at the pressure outlet faces, and this static pressure at the outlet faces is often assumed to be atmospheric pressure (zero-gauge pressure) [37].

The simple pressure-velocity coupling method was used to perform all the simulations. The convergence criteria used was a residual of 10^{-5} , as also used elsewhere [21]. In addition, second-order spatial discretization has been used for pressure and gradient terms. Equations for momentum, turbulent kinetic energy, and specific dissipation rates have all been solved using second-order upwind methods.

2.3. Mathematical and turbulence modeling

In computational fluid dynamics (CFD), the governing equations of fluid dynamics are solved using numerical techniques and algorithms. The governing equation of the computational domain describes the three main concepts of conservation: conservation of energy, conservation of momentum, and conservation of mass (continuity) [35,36].

conservation of mass (continuity Equation) [36].

Table 2
Boundary conditions for the presented work.

<u>NO</u>	<u>Boundary type</u>	<u>Boundary conditions</u>	<u>Boundary Values</u>
1	Inlet Velocity(U_{in})	Inlet- $4.5 \frac{m}{s}$	4.5 (m/s)
2	Pressure	Outlet-	Zero-gauge pressure
3	Walls	walls	-

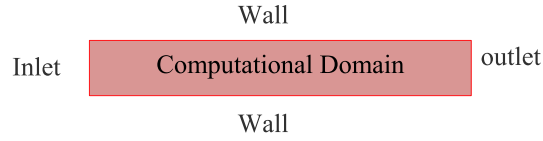


Fig. 16. Boundary condition for simulation work [37].

$$\frac{\partial \rho}{\partial t} + \frac{\partial}{\partial x_i} (\rho u_i) = 0 \quad (1)$$

Momentum Equation [36].

$$\frac{\partial}{\partial t} (\rho u_i) + \frac{\partial}{\partial x_j} (\rho u_i u_j) = -\frac{\partial p}{\partial x_i} + \frac{\partial \tau_{ij}}{\partial x_j} \quad (2)$$

Energy equation [36].

$$\frac{\partial}{\partial t} \left[\rho \left(h + \frac{1}{2} u_i^2 \right) \right] + \frac{\partial}{\partial x_j} \left[\rho u_j \left(h + \frac{1}{2} u_i^2 \right) \right] = \frac{\partial p}{\partial t} + \frac{\partial}{\partial x_j} \left(u_i \tau_{ij} + \lambda \frac{\partial T}{\partial x_j} \right) \quad (3)$$

where the following formulas are used to define the stress tensor and enthalpy h [35,35]:

$$\tau_{ij} = \mu \left(\frac{\partial u_i}{\partial x_j} + \frac{\partial u_j}{\partial x_i} \right) - \frac{2}{3} \mu \frac{\partial u_i}{\partial x_i} \delta_{ij} \quad (4)$$

$$h = C_p T \quad (5)$$

A connected non-linear partial differential equation system represents six indeterminate flow-field variables: U, V, W, P, T, and ρ . These equations are given as five above.

Most flows found in natural and industrial systems are classified as turbulent. A viscous fluid flow's chaotic and unpredictable motion is called turbulence. Varying velocity, pressure, and temperature fields define turbulent flows, as in Refs. [35,36].

Due to their small size and high frequency, these oscillations are too computationally expensive and complex to replicate directly in real-world engineering applications. Therefore, turbulence models are needed to calculate these parameters in terms of predefined numbers.

The following categories can be used to group the turbulence modes.

- (1) Reynolds-Averaged Navier-Stokes (RANS) equations-based models
- (2) Large eddy simulation (LES)
- (3) Detached eddy simulation (DES) and other hybrid models
- (4) Direct numerical simulation (DNS)

The Reynolds-Average Navier-stroke (RANS) models manage the transfer of the averaged flow quantities among the turbulence models, considerably lowering the computing work. These are frequently used in real-world engineering applications.

Shear-stress Transport (SST) $k-\omega$ turbulence Model.

The transitional $k-k\ell-\omega$ model and the shear-stress transport (SST) $k-\omega$ model for separated and transitional flows. Both of them have benefits and drawbacks. For a more extensive class of flows (transonic flows, flows with an adverse pressure gradient, etc.), the SST k -model is more accurate and dependable than the regular k -model [35].

Two transport equations for the specific dissipation rate (ω) and the turbulent kinetic energy (k) form the SST $k-\omega$ model [35,35].

$$\frac{\partial}{\partial t} (\rho K) + \frac{\partial}{\partial x_i} (\rho K u_i) = \frac{\partial}{\partial x_j} \left(\Gamma_k \frac{\partial k}{\partial x_j} \right) + \tilde{G}K - Y_k + S_k \quad (6)$$

$$\frac{\partial}{\partial t} (\rho \omega) + \frac{\partial}{\partial x_i} (\rho \omega u_i) = \frac{\partial}{\partial x_j} \left(\Gamma_\omega \frac{\partial \omega}{\partial x_j} \right) + G_\omega - Y_\omega + D_\omega + S_\omega \quad (7)$$

Where, $\tilde{G}K$ is the result of mean velocity gradients producing turbulent kinetic energy.

G_ω Represents the generation of ω . Γ_k and Γ_ω Represents the effective diffusivity of k and ω . Y_k and Y_ω Represent the dissipation of k and ω due to turbulence. D_ω Represents the cross-diffusion term, S_k and S_ω Represents the user-defined source term,

Especially in this paper, since there is flow separation created from the wall of the diffuser, fluid flows away from the wall or free stream fluid away from the wall and approaching the wall is best treated in the SST k -omega model as has been used in Refs. [21,30,30,38,39] to control the effects of separation of fluid from the wall of diffuser surfaces. The simulation empty diffuser model studies [16,31] were used to determine the optimum parametry fo diffuser. The SST K -omega model extracts the results independent of free stream volumes [21].

A pressure-based solver type, a steady state with an SST k-omega model, and air fluid flowing over and inside the diffuser were used for the simulation throughout this work.

2.4. Mesh independence test

The standard method to test this grid independence is to increase the resolution (increase the number of elements and nodes) and repeat the simulation until the result becomes independent of the grid size [37]. It is known that finer mesh sizes give more accurate and stable results. However, more computational time and cost are incurred as the mesh gets finer. Results pertinent to different mesh sizes generated in this work were compared below to test the deep impact of mesh size on CFD results at the diffuser outlet. As shown in Fig. 17, comparing the non-dimensional velocity (velocity at a given point over inlet velocity) with the number of meshes, the finer mesh size of 1,416,177 elements (finer mesh) produces the same results as those for smaller mesh sizes; hence, a finer mesh of 1416177 elements was selected to save computational time and resources.

As shown in Fig. 17, U/U_{in} stands for velocity divided by inlet velocity (inlet wind velocity).

3. Results and discussion

3.1. Design parameters and shape of the diffuser

In optimizing the performance of diffuser-augmented wind turbines, evaluating the design parameters of the diffuser was critical in finding a sound power output, increasing the efficiency for low wind speeds, and understanding the optimal parameters for placing a wind turbine inside the diffuser to achieve high power output. Studying diffuser parameters without the wind turbine is necessary as a baseline, even though the integral system simulation can reveal interactive effects. The parameters studied here to get optimum diffuser parameters were the opening angle of the diffuser, flange height, inlet shroud, flange angle, and different diffuser shapes considered. The 3D flow simulation gives detailed information on the flow inside and outside diffuser surfaces. The graphs and contour plots were constructed using non-dimensional and dimensional methods.

The non-dimensional velocity (velocity ratio), calculated using fluid velocity at a given point over inlet velocity, compares the velocity contour shown in Fig. 20, Fig. 21, Fig. 22, and Fig. 24.

The other left figures were analyzed in terms of rate using dimensional speed to visualize the comparison. The location of the input data for generating the graph and plots is indicated after each figure accordingly.

3.1.1. opening angle study of flat diffuser

In addition, from the bottom of the diffuser wall to the upper border of the diffuser with the help of line and plane, as explained below.

Fig. 18 considers studies on opening angles from 2° to 22° , extending from the horizontal to the positive y-axis. Throughout the study, we utilized non-dimensional velocity (variable velocity in the x-axis divided by inlet velocity (4.5 m/s)) along the y-axis plot and non-dimensional length (length from -1.35 m to 4.05 m divided by the length of the diffuser (0.9 m)) along the x-axis. Fig. 18 demonstrates the effect of the opening angle on the velocity ratio, which rises to a maximum at 8° and then begins to fall from 10° onwards. A maximum velocity of 6.57 m/s, or 1.444 non-dimensional velocities, was attained inside the diffuser, as shown in Fig. 20. The rate inside the diffuser increased by 46% from 4.5 m/s inlet velocity to 6.57 m/s (1.444). On the central axis of the diffuser, a speed of 6.13 m/s was recorded at an angle of 8° for locations of (0.217 or 0.195 m) and (0.238 or 0.214 m) from the inlet of the diffuser length. The velocity is shown along the y-axis. The y-axis ($\frac{y}{D}$) was sketched at 0.195 m from the input data of the bottom (-0.36 m) to the upper wall of the diffuser of 0.36 m, shown below; Fig. 19 indicates that the rate inside the diffuser creates top speed at an 8° opening angle.

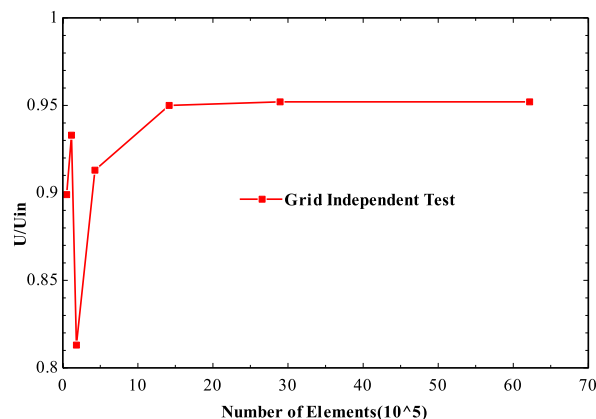


Fig. 17. Grid-independent test.

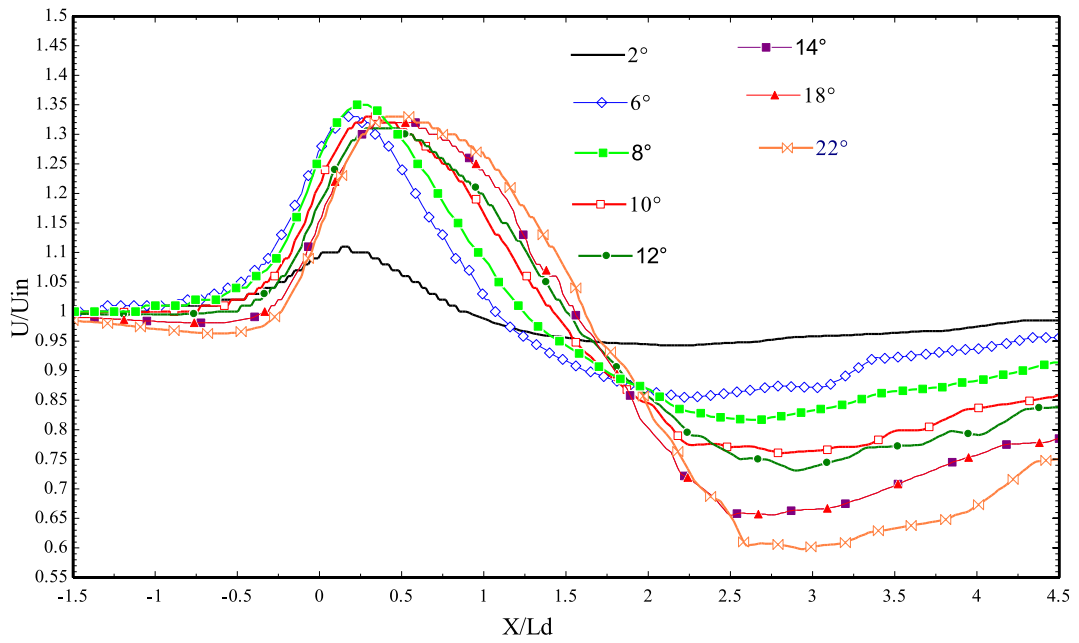


Fig. 18. Compare velocities for different opening angles of the flat diffuser at the center.

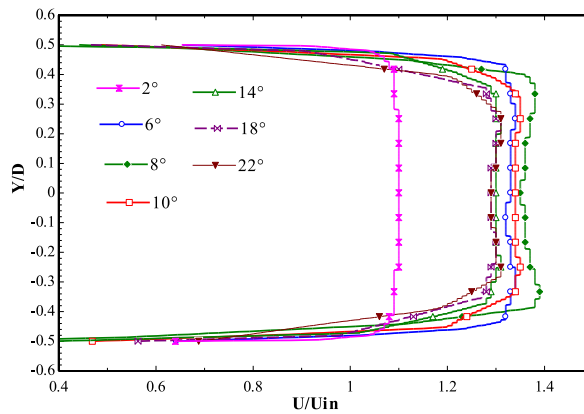


Fig. 19. Non-dimensional velocity comparison with the opening angle of a flat diffuser along the y-axis.

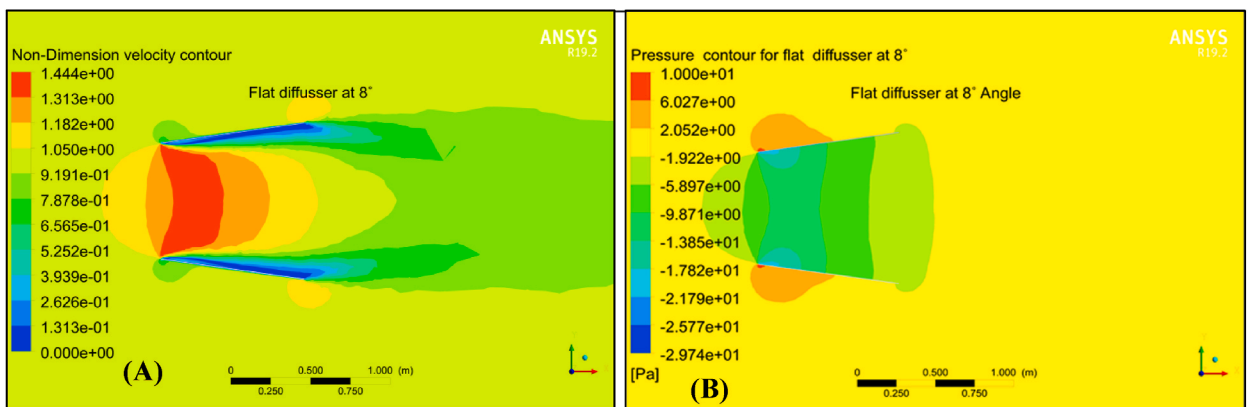


Fig. 20. Non-dimensional velocity (A) and pressure contours (B) for the flat diffuser at an 8° opening angle.

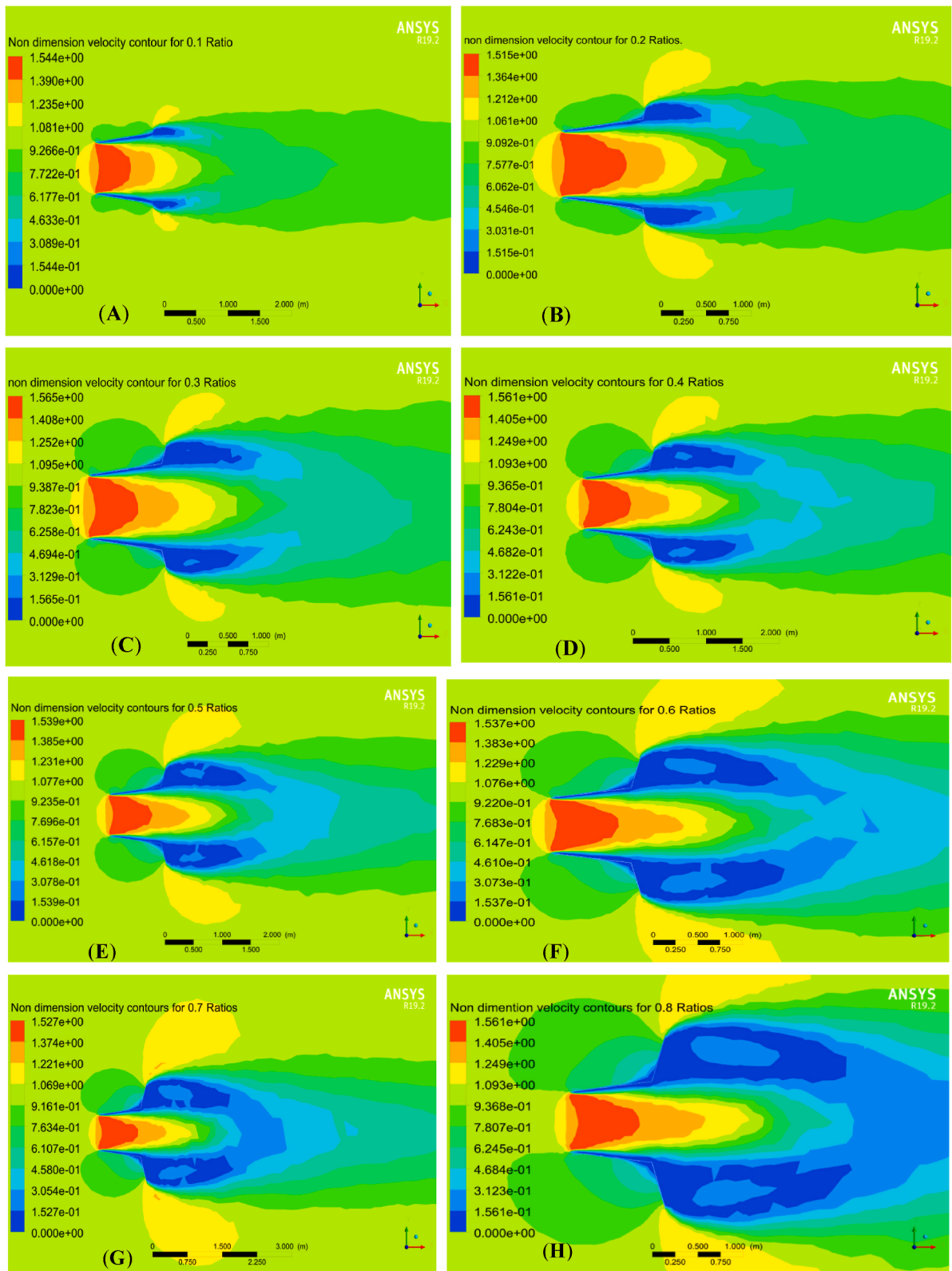


Fig. 21. Non-dimensional Velocity contours for 0.1 to 0.8 flange ratios for a flanged flat diffuser on a central plane.

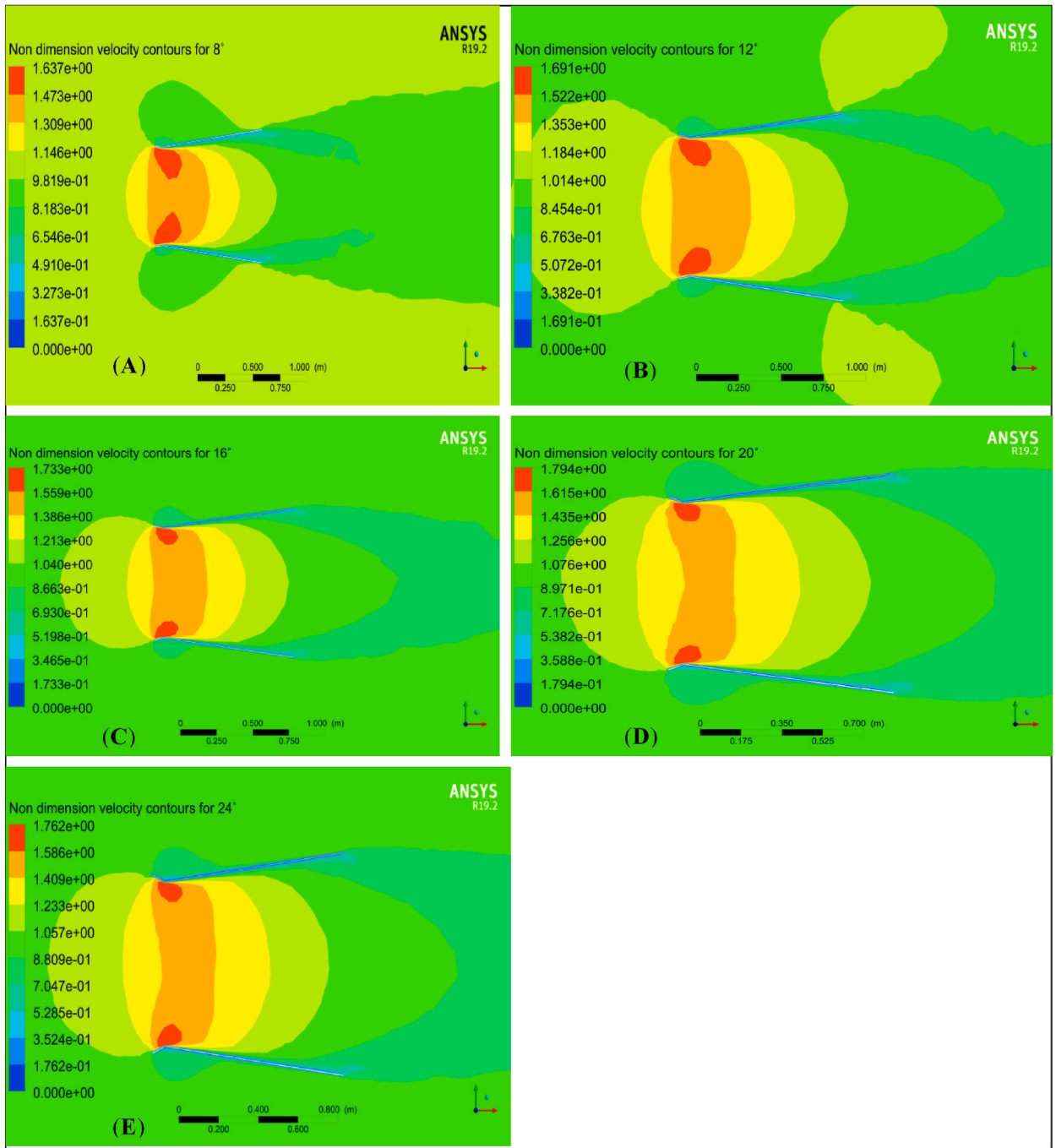


Fig. 22. Non-dimensional Velocity contour for inlet shroud flat diffuser at inlet shroud angle variation from 8° to 24°.

For velocity contours indicated in Fig. 20, the velocity is increased inside the diffuser for some length, reaches a maximum, and starts to decrease on account of continuity. When it exits the enclosure, the velocity becomes nearly the same as the free stream velocity at the inlet to the chamber. A non-dimensional velocity contour, obtained by dividing the speed of the contour by the inlet velocity, was drawn to create Fig. 18(A). By dividing the maximum velocity contour (6.57 m/s) by the inflow velocity (4.5 m/s), the system achieved a maximum velocity ratio of 1.444. The same trend was used for the entire non-dimensional velocity contour below.

3.1.2. Flange height ratio study of flanged flat diffuser

When the air moves through the diffuser wall internally or externally at a speed of 4.5 m/s, high velocity is produced at the diffuser entrance locations. The diffuser's rear creates a low pressure that, combined with the diffuser's flange, draws more wind into the

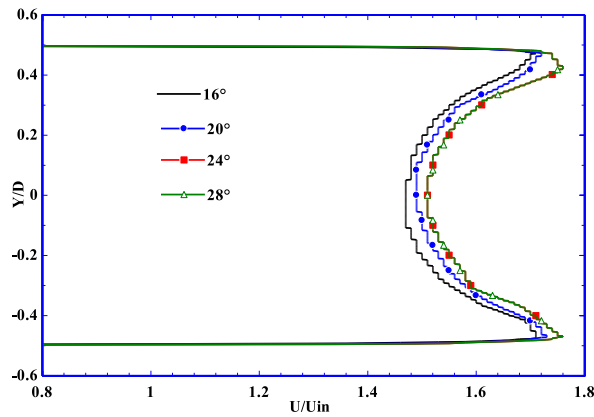


Fig. 23. Non-dimensional velocity at the inlet of diffuser for inlet-shroud-flanged flat diffuser at different inlet shroud angles.

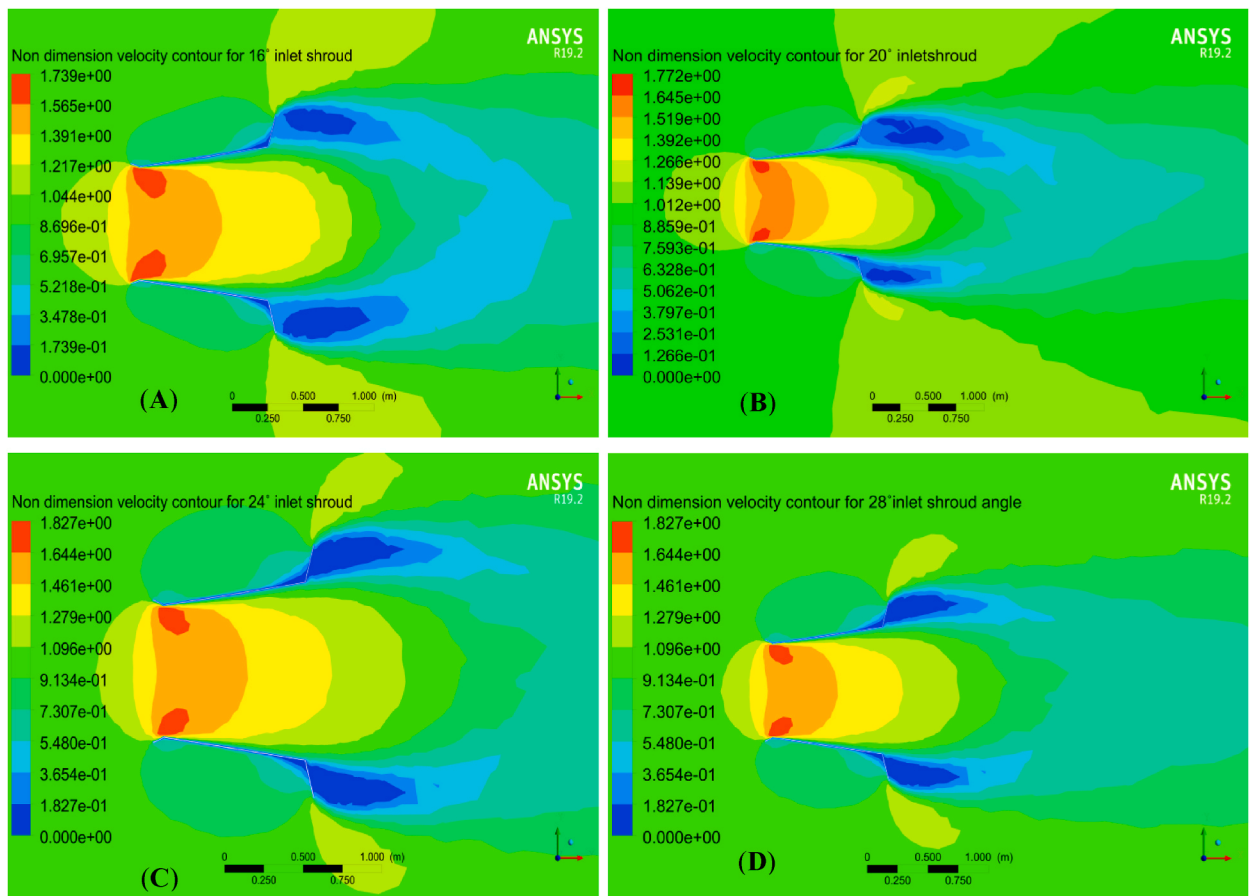


Fig. 24. Non-dimensional velocity contour along the central plane for the inlet shroud-flanged flat diffuser at different inlet shroud angles.

diffuser. In this instance, the flange’s primary function is to generate the vortex at the diffuser’s back and reduce pressure. So the formation of low pressure at the back of the diffuser causes the wind to be sucked at high speed into the diffuser.

The effect of flange height variation on velocity change through the internal and external flat diffusers is presented in Fig. 21 for the maximum diffuser opening angle of 8°. The non-dimensional velocity is compared with ratios of the diffuser flange length. It is clearly shown in Fig. 21 that the velocities were maximum at the inlet region of the diffuser and decreased when moving to the right of the diffuser flange height to the minimum.

The velocity at the diffuser entrance increases and reaches its maximum at the flange height-throat ratio of 0.3. The flow separation

is generated after this ratio. This may disrupt the flow through wind turbines. For this reason, the flange height ratio of 0.3 is the best for maximizing and managing the extra size and cost.

Compared with a 0.3 flange ratio, a 0.1 flange ratio had less speed through the diffuser.

Lower velocity was observed for the second flange ratio of 0.2 compared to the first and third ratios. In addition, the 0.3 ratio has much more speed through the diffuser than all the flange ratios, from 0.1 to 0.8. Since the low-pressure creation at the diffuser rear causes more wind to be drawn into the diffuser inlet areas at a speed of (1.565 velocity ratio) or 7.083 m/s, adding a flange to the diffuser's end enhances the velocity at the entrance of the diffuser. The flange height ratio of 0.3 contributes 57.3% of the velocity increment from the inlet velocity of 4.5 m/s, or the flange addition contributes to the velocity increments of approximately 46%–57.3%, or 11.3% improvement. It is reasonable that adding the flange also contributes to the velocity increments, similar to the opening angle effect, and confirms the work of [16,21], and [22].

3.1.3. Inlet shroud angle study for inlet-shrouded flat diffuser

A small inlet shroud, 0.1 times the inlet diffuser diameter, was added to the inlet section to collect enough air into the diffuser and to optimize the velocity inside the diffuser. Then, The work analyzed the effect of the inlet shroud angle shown in Fig. 22 to determine the maximum speed inside the diffuser.

Investigations were conducted on the inlet shroud angles from 8° to 24° at 4° intervals. The velocity rises as the inlet shroud angle increases from 8° to 20°, and the maximum rate of 1.794 velocity ratio is observed for the 20° inlet shroud angle and decreases for 24° inlet shroud angles; see Fig. 22.

But this velocity increment is obtained close to both side walls of the diffuser, which means around the tip of the blade; it is essential to extend this advantage to the whole internal diameter of the diffuser to get enough wind velocity and install the wind turbine inside the diffuser. Then, the following section discusses the combined effect of flange height and inlet shroud angle.

3.1.4. Inlet shroud angle study for inlet-shroud-flanged flat diffuser

Fig. 21 reveals that a 0.3D constant height of the flange and a small constant inlet shroud length of 0.1D resulted in the realization of the maximum velocity. Furthermore, Figs. 23 and 24 examine and discuss the combination of variable inlet shroud angle and constant flange height.

The non-dimensional velocity contours in Fig. 24 illustrate the velocity through and at the diffuser's intake. The non-dimensional velocity contour is used while comparing the impact of inlet shroud angles at 16°, 20°, 24°, and 28°. Among these angles, the speed increased from 16° to 24° and remained constant for both 24° and 28°, which is the same for Fig. 23.

In Fig. 23, $\left(\frac{Y}{D}\right)$ indicates the ratio of the length along the y-axis by the diffuser's inlet diameters from the bottom of the diffuser to the upper diffuser wall and $\left(\frac{U}{U_m}\right)$ represents the ratio of velocity along the y-axis (velocity by inlet velocity), which is drawn along the x-axis.

It is evident from the results shown in Figs. 23 and 24 that the 24° inlet shroud angle can be taken as the optimum angle, which produces maximum velocity at the inlet of the diffuser. The speed is zero at the bottom wall. It keeps increasing, reaching a maximum of 7.91 m/s (1.76 velocity ratio) at −0.45 non-dimensional length, and to a small extent, the velocity decreased in the center and kept growing to 7.91 m/s (1.76 velocity ratio) at 0.45 non-dimensional length and reduced as it reached the wall where the speed is zero at the top and bottom of the diffuser.

Generally, a maximum velocity of 8.23 m/s was obtained inside the diffuser in the case of the inlet-shroud-flanged flat diffuser, as shown in Fig. 25.

The velocity increases from the diffuser's center to the diffuser's wall [16], and when it reaches the wall, it reduces to zero. Maximum speed is displayed closer to the wall of the diffuser. This maximum velocity produced away from the wall helps the blade to

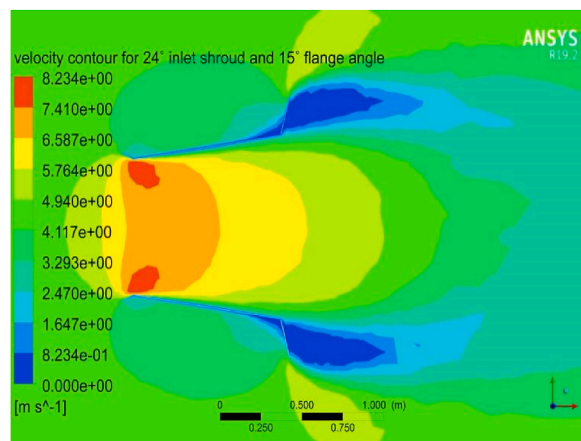


Fig. 25. Maximum velocity contour for optimum parametric study of the inlet shroud-flanged flat diffuser.

rotate fast and the wind turbine to generate more power from an inlet velocity of 4.5 m/s. The results obtained in Fig. 25 above were the summation of the results of the optimum flange height study achieved at ($\frac{H}{b} = 0.3$), the inlet shroud angle obtained at (24°) angle (with flange), and the inlet opening angle obtained at (8°).

3.1.5. Inlet shroud-flanged- flat diffuser (zero and 15 flange-angle comparison)

Comparing the flange angles of zero and 15° , as seen in Fig. 26 below, a 15° flange angle produces a higher velocity in the inlet section of the diffuser all along the diffuser cross-section. Hence, using the 15° flange angle compared to the zero angles is reasonable and agrees with the previous work [22].

3.2. Parametric study on diffuser shapes

3.2.1. Forward upper stepped diffuser and forward lower stepped diffuser comparison

As can be seen in Figs. 27 and 28, the forward lower-stepped diffusers with similar inlet and outlet diameters had the maximum velocity, surpassing the forward higher-stepped diffuser.

Forward lower-stepped diffuser features produce top speed and minimum pressure in the middle of the diffuser due to the inverse relationship between pressure and velocity from Bernoulli's principle (see Fig. 29). As illustrated in Fig. 27, both the forward upper and lower-stepped diffusers attain maximum speed at 8° , like that of the flat diffuser.

This maximum velocity for the forward lower stepped diffuser ranges from 5.8 to 6.261 m/s, as shown in Fig. 28 (right). Hence, compared with the inlet velocity of 4.5 m/s, the forward lower-stepped diffuser produces a 39.133% increase from the previous inlet velocity.

The non-dimensional velocity (left) and pressure coefficient (right) portions are contracted in Fig. 29. From the inlet, the speed rises to its maximum, and then for both upper and lower stepped features, more specifically, the lower-stepped features reach their maximum velocity (see Table 3). The speed increases from the inlet and reaches the maximum, then decreases for lower and upper-stepped features; precisely, the lower-stepped one attains maximum velocity and lower pressure. As can be noticed in Fig. 29, the pressure was lower for the forward lower step than the upper step due to the impact of the lower-stepped shape on the flow field.

3.2.2. Side-stepped (lower side and upper side) diffuser parametric study

The velocities are compared in Fig. 30 for the lower and upper side-stepped diffusers at the optimum opening angle of 8° ; the maximum velocity was produced for the lower side-stepped diffusers. Similarly, as Fig. 30 makes abundantly evident, pressure was highest for the side upper stepped diffuser and lower for the side lower stepped diffuser due to the inverse relationship between pressure and velocity. The impact of the decrease in pressure and increase in velocity for side lower stepped diffuser has happened for the side lower stepped towards increasing the flow speed and lowering pressure. Then, this type of side-stepped diffuser is advantageous for more investigation to add to flange parts; a lower stepped advantage was taken and added to the flange part of the diffuser, as shown below in Fig. 31, and produced maximum power output.

3.2.3. inlet shrouded side lower stepped flange diffuser parametric shape study

More velocity is created inside the diffuser around the entrance in this instance than in any of the other stated examples, and the flange portion is side-stepped. Then, it was determined that the ideal diffuser for installing wind turbines was the intake inlet-shrouded-side-lower stepped flange diffuser.

As stated in Fig. 31 below, the XY plane is parallel to the flow direction of the wind from the left to the right of the flange exit direction. It is clearly shown that a high-pressure drop is created at the exit section of the curved flange due to the flange shape advantages that make the flow more turbulent, as shown in Fig. 33 below. More pressure reduction makes the fluid flow be returned inside the diffuser to the inlet section, which results in higher velocity at the inlet section of the diffuser.

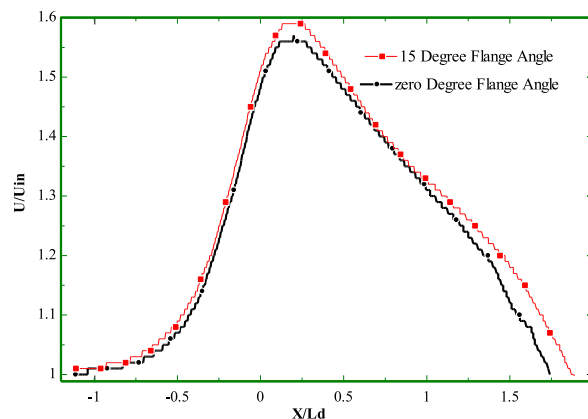


Fig. 26. Effects of the flange angle on the velocity profile inside the inlet shroud-flanged flat diffuser.

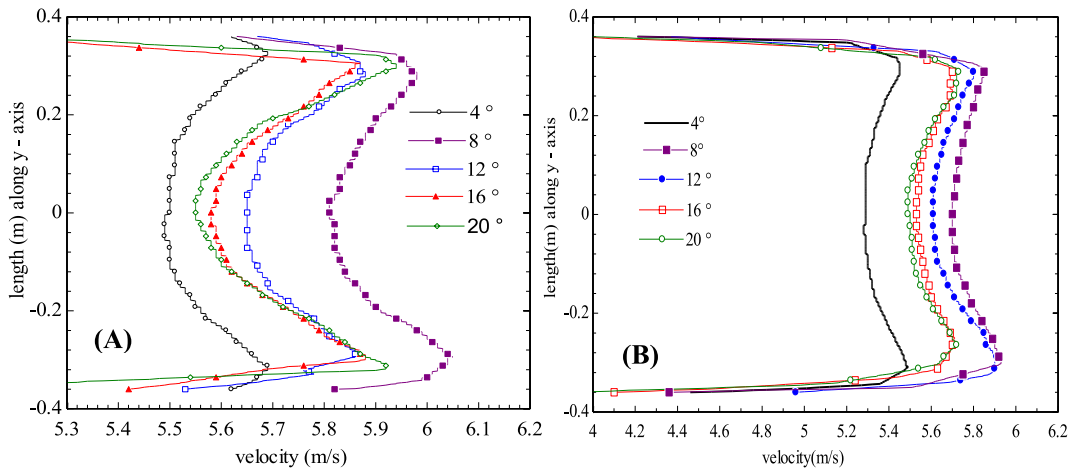


Fig. 27. Velocity profile for forward lower stepped diffuser (A) and forward upper stepped diffuser (B) at various opening angles.

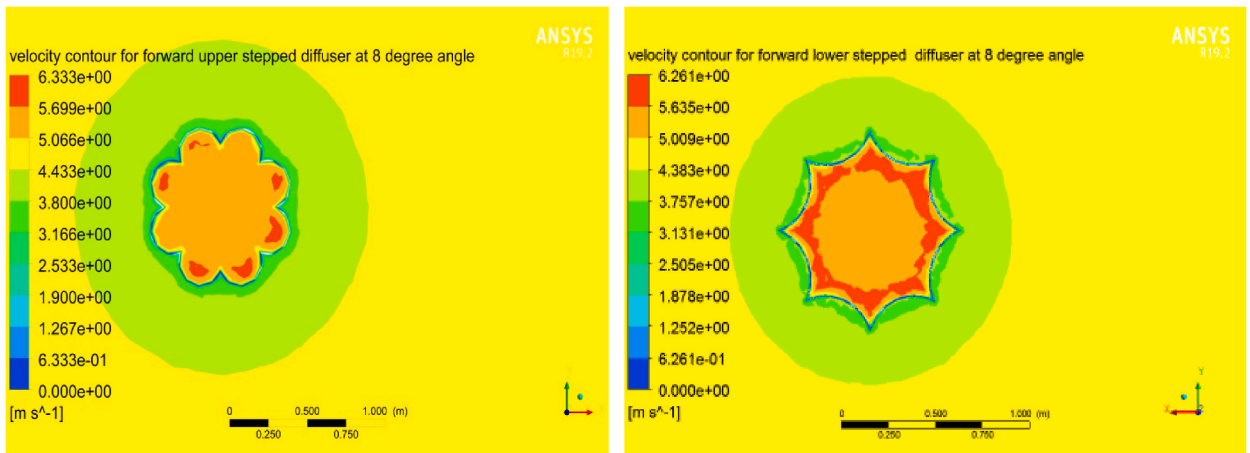


Fig. 28. The diffuser velocity contours with stepped at different opening angles, both upper and lower.

The flow is separated from the stepped flange section, which increases the inlet section wind speed of the diffuser, as can be observed in Fig. 31 (a, b, and c). From 4.5 m/s of inlet average wind speed, 9.12 m/s of maximum velocity was generated by the inlet shrouded stepped flange diffuser with top velocity increments of 102.66%, which is also in agreement with the previous studies [14].

As clearly indicated in Fig. 31, a more significant portion of the inside diffuser section is concentrated, with an average velocity ranging from 7.2 m/s to 8.2 m/s, which is more suitable for wind turbine installation (with 82.2% velocity increments). Hence, this velocity increment might help advance the state of wind turbine technology. In 2030, 20% of the world's electricity might theoretically come from wind energy [40].

The maximum velocity attained in the center of the diffuser was 7.55 m/s at 0.175 m from the inlet of the diffuser (inside inlet shrouded-side stepped flange diffuser), as shown in Fig. 32.

Hence, the wind turbine installation could be recommended where high wind speed occurs at 0.175 m from the inlet of the diffuser. The optimized diffuser shape was shown to have an optimal velocity for the same input of 4.5 m/s intake velocity. The air velocity increased from the intake up to 0.175 m in length and kept up at this rate, declining to the minimum afterward as it moved from left to right in the inner and outer sections of the diffuser.

The vortex that developed at the diffuser's rear caused the maximum velocity to be created at the inlet section areas. Because of the flange shape advantage, the turbulent kinetic energy was greatest around the vortex generation areas, as shown in Fig. 33.

A - inlet-shrouded flat flange diffuser, and **B** - inlet-shrouded-side stepped flange diffuser.

In contrast to the inlet shrouded-flange flat diffuser and flat diffuser, the inlet shrouded-flange side-stepped diffuser produced a maximum velocity and lower pressure surrounding the diffuser's inlet, as illustrated in Fig. 32 and Table 4

As indicated below in Fig. 33, the turbulent kinetic energy created was maximum on the outside of the diffuser exit flange, which reduces the pressure, and the same value of turbulent kinetic energy was observed at minus 1 m and at 3 m length of the enclosure, implying the enclosure has no impact on the result of the work.

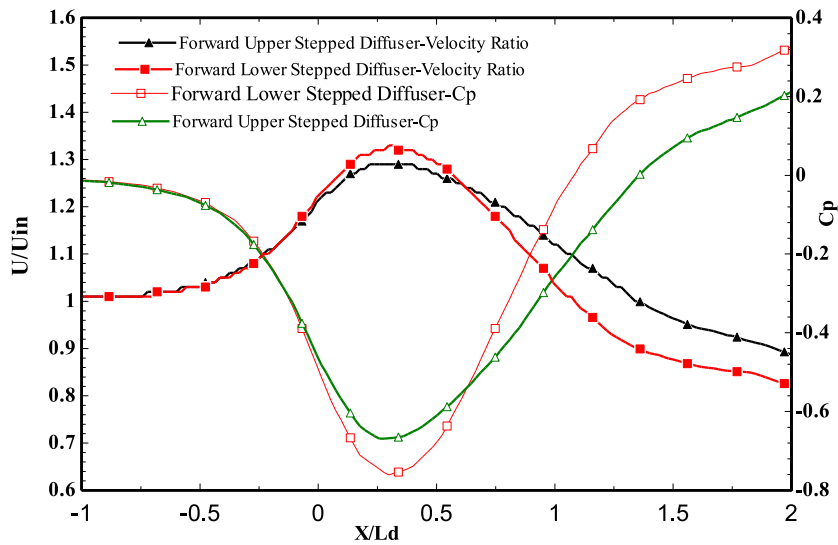


Fig. 29. Velocity ratio and pressure coefficient for forward-lower and forward-upper stepped diffuser at 8°.

Table 3
Maximum velocity comparison for both forward upper and lower stepped diffuser.

Diffuser type	Diffuser Angle	Inlet	Maximum velocity along the y-axis.	% increments concerning inlet velocity
Forward lower stepped	8°	4.5 m/s	6.04 m/s At -0.3 m	34.22%
Forward upper stepped	8°	4.5 m/s	5.93 m/s At -0.3 m	31.78%

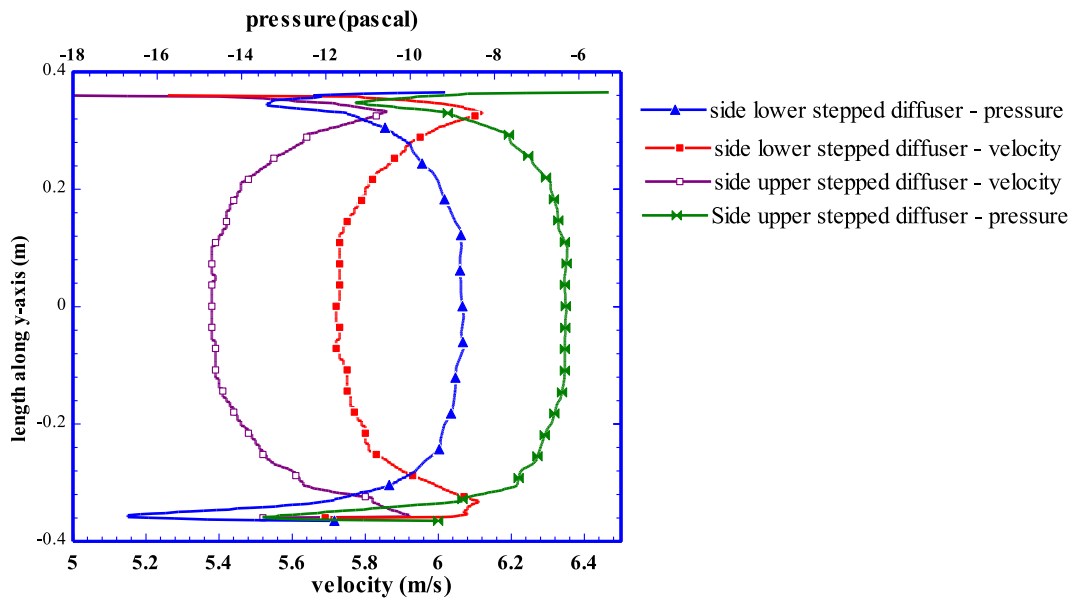


Fig. 30. Comparison of lower and upper-side stepped diffusers regarding pressure and velocity.

Table 5 compares the present work with the previous works of literature by comparing the velocity output obtained concerning their inlet velocity. The current work shows advanced results.

Fig. 34 above compares the opening and inlet shroud angles with the targeted non-dimensional velocity increments. The opening angle was taken from 4° to 18°, and the inlet shroud angle was from zero to 24°. The result of the study shows, as observed in the figure above, that a smaller increment of velocity, about 5.95 m/s or $\frac{U}{U_{in}} = 1.324$, was shown when the inlet shroud angle was zero on the x-axis line. After an increment in the inlet shroud angle from zero to 24° and the opening angle at 8°, a large increment in velocity ratio is

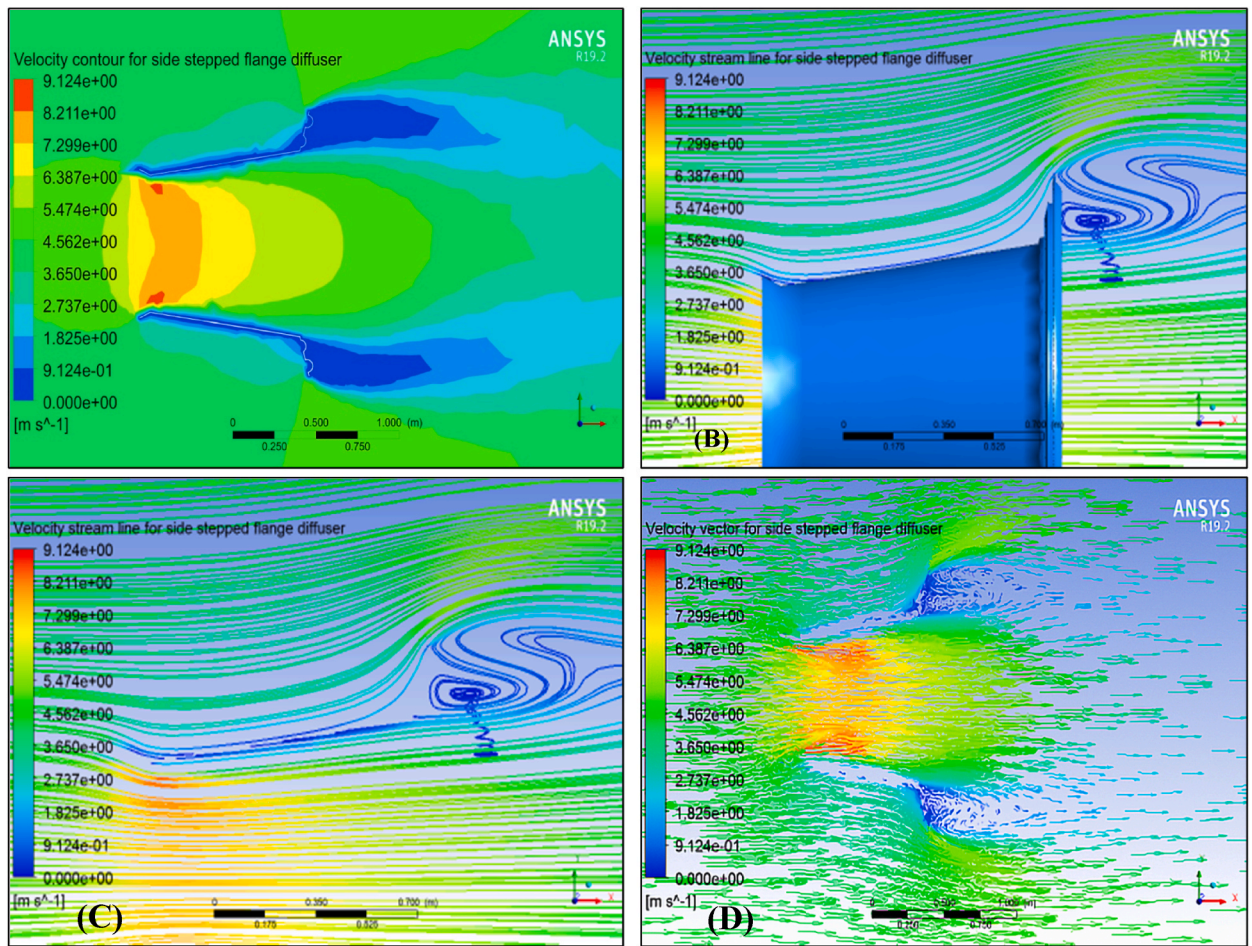


Fig. 31. Velocity contours, velocity streamlines, and velocity vectors for the inlet shrouded lower stepped flange diffuser.

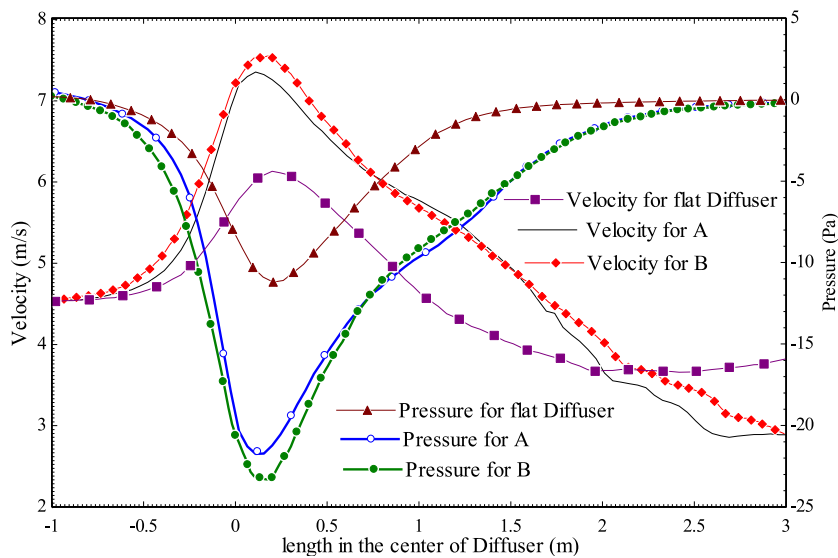


Fig. 32. Comparison of velocity and pressure for inlet-shrouded flat flange diffuser, inlet-shrouded-side stepped flange diffuser, and flat diffuser.

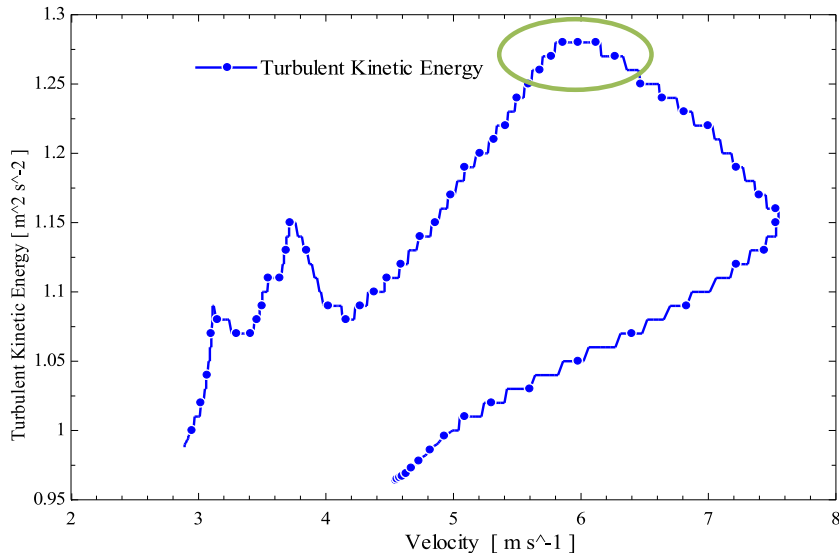


Fig. 33. Turbulent kinetic energy for the inlet-shrouded side-lower stepped flange diffuser.

Table 4

Comparison of all diffuser types in terms of efficiency.

Diffuser type	Angle			Inlet velocity	Maximum velocity(m/s)	% increments about an inlet.	
	Inlet-shroud	Diff. inlet Opening angle	Flange			Velocity (%)	Power (times)
Flat	NO	8°	NO	4.5 m/s	6.57	46 %	3.11
Flanged flat	24°	8°	0°		7.083	57.4 %	3.89
Inlet-shroud-flange flat	24°	8°	15°		8.234	82.97 %	6.12
Forward lower stepped	NO	8°	NO		5.85	30 %	2.2
Side lower stepped	NO	8°	NO		6.646	47.7 %	3.22
Inlet-shrouded side-stepped flange	24°	8°	15°		9.124	102.75 %	8.33

Table 5

Comparison of the present studies with the previous studies.

Different researchers	Inlet velocity (m/s)	Output velocity(m/s) Av.max(maximum)	Percent increase in velocity about inlet velocity.	Increment in power
Lokesharun et al. [41].	5	7.62(8.017)	52.4%(60.34)	3.54
Parsa and Maftouni, [21].	8	12	50%	3.375
Bekele and Bogale, [16].	5	7.69	53.8%	3.64
Present study	4.5	8.6675(9.124)	92.61%(102.76%)	7.146

observed. Hence, at an opening angle of 8° and an inlet shroud angle of 20°, a maximum velocity ratio of 1.794 has resulted.

3.3. Result validation

The methodology used in this work was validated using the experimental work of [26] for the diffuser structure of an inlet diameter of 12 cm, an outer diameter of 24 cm, and a length ratio of $\frac{L}{D} = 7.7$, and compared with simulation results generated for the same dimensions.

In Fig. 35, U/UFstrm stands for non-dimensional velocity, the ratio of velocity over free stream velocity, and X/L stands for non-dimensional length in the x-direction over the length of the diffuser. The simulation results obtained by using an enclosure diameter of 10 m and length of 11 m show the same trend with fairly good agreement with the experimental work of Ohya et al. [26,42] for the height of 2 m, width of 3 m, and 15 m length rectangular cross-section with a maximum error of 4.47%. In this comparison, the difference between the previous experimental work and this work might be attributed to the surface roughness effects. The advantage of excessive enclosure length and diameter in this study is that it reduces the impact of wall turbulence creation, resulting in a lower velocity than in the experimental work.

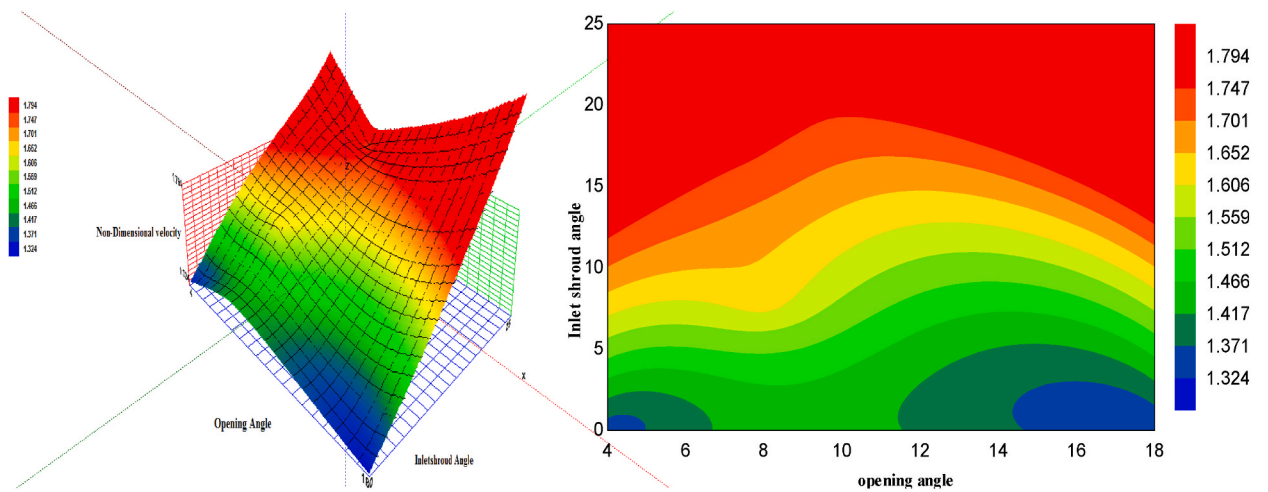


Fig. 34. Compares the opening angle and inlet shroud angle using a surface plot (left) and gradient plot (right) to non-dimensional velocity (velocity ratio).

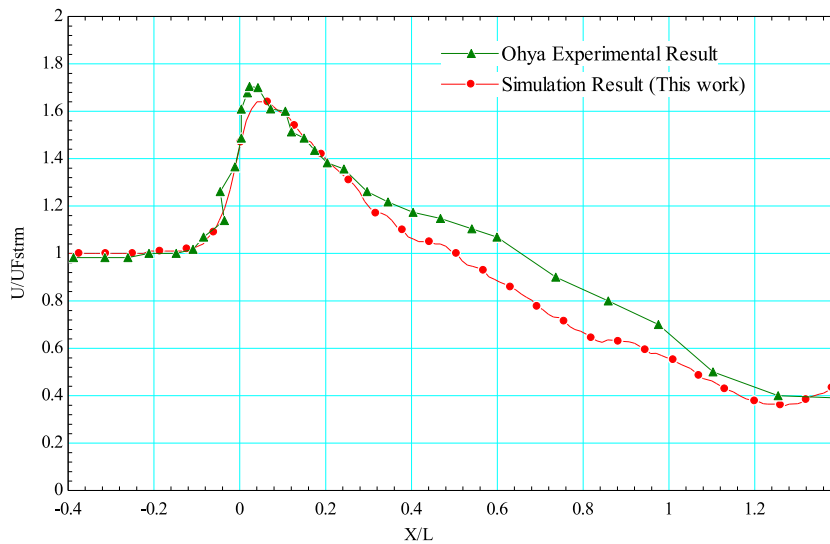


Fig. 35. Comparisons of the simulation results of this study with the experimental results of Ohya et al. [26].

4. Conclusions

This research investigated the optimum parameters and shape of a diffuser for increasing the power output of wind turbines using the CFD approach.

Different parametric effects of the diffuser, shapes, size, and comparative results were discussed and analyzed. Many diffuser options were modeled and imported to ANSYS FLUENT to analyze each parametric effect on the diffuser performance. The winglet-like structure (lower side-stepped flanged) at the exit section of the diffuser was observed. Effects concerning velocity changes inside the diffuser have been analyzed and discussed.

In conclusion, the following are the significant findings of the current research.

Maximum velocity can be achieved at an 8° opening angle from the range studied (2°–22°), contributing 46% of the velocity increment from the inlet velocity. The additional flange at the exit of the diffuser contributes 57.4% of the velocity increment at 0.3D flange height in the ratios of 0.1–0.8 range explored. With a 15° flange angle, the inlet shroud addition to the diffuser contributes to the increment in velocity at the inlet tip section of the diffuser by about 87.2%.

Among the forward upper/lower stepped and the side upper/lower stepped shapes of the diffuser, the side lower stepped creates maximum velocity inside the diffuser. The optimal velocities, averaging 8.67 m/s and reaching a maximum of 9.12 m/s, demonstrated substantial increases of 92.61% and 102.7%, respectively. Attaining these optimum conditions involved adjusting the inlet shroud,

opening angle, flange angle, flange height ratio, and stepped shape and integrating a lower side-stepped flange shape into the diffuser. However, the advancement of this work is hindered by the scarcity of limited financial resources and a shortage of experimental tools necessary for its implementation.

Hence, further work system simulation of the lower-side stepped flange shape of the diffuser with the wind turbine, experimental investigation of multi-objective optimization of the diffuser shape, and experimental field testing are suggested as a way forward.

Data availability statement

The data that has been used is confidential.

CRediT authorship contribution statement

Debela Alema Teklemariyem: Conceptualization, Formal analysis, Investigation, Methodology, Project administration, Resources, Software, Supervision, Validation, Visualization, Writing – original draft. **Eshetu Tadesse Yimer:** Investigation, Methodology, Software, Validation, Visualization, Writing – review & editing. **Venkata Rammaya Ancha:** Data curation, Formal analysis, Methodology, Software, Supervision, Validation, Visualization, Writing – review & editing. **Balewgize Amare Zeru:** Conceptualization, Formal analysis, Methodology, Project administration, Supervision, Validation, Writing – original draft, Writing – review & editing.

Declaration of competing interest

The authors declare that they have no known competing financial interests or personal relationships that could have appeared to influence the work reported in this paper.

Acknowledgments

Partial support from JiT Center of Excellence is gratefully acknowledged.

References

- [1] I.E.A. International, E. Agency, Renewable Energy Market Update, 2023.
- [2] I. Renewable, E. Agency, Renewable Energy and Jobs Annual Review (2022) 2022.
- [3] P.-E. Morthorst and S. Awerbuch, "The Economics of Wind Energy."
- [4] R. Bontempo, M. Manna, Diffuser augmented wind turbines : review and assessment of theoretical models, *Appl. Energy* 280 (September) (2020) 115867, <https://doi.org/10.1016/j.apenergy.2020.115867>.
- [5] R. Bontempo, M. Manna, On the potential of the ideal diffuser augmented wind turbine : an investigation by means of a momentum theory approach and of a free-wake ring-vortex actuator disk model, *Energy Convers. Manag.* 213 (March) (2020) 112794, <https://doi.org/10.1016/j.enconman.2020.112794>.
- [6] M. J. W, W.M.P. Jr, *Technical Notes* 24 (5) (2008) 1–5, <https://doi.org/10.2514/1.37134>.
- [7] R. Bontempo, M. Manna, Performance analysis of open and ducted wind turbines, *Appl. Energy* 136 (2014) 405–416, <https://doi.org/10.1016/j.apenergy.2014.09.036>.
- [8] D. Allaei, Y. Andreopoulos, Invelox : description of a new concept in wind power and its performance evaluation, *Energy* (2014) 1–9, <https://doi.org/10.1016/j.energy.2014.03.021>.
- [9] D. Allaei, D. Tarnowski, Y. Andreopoulos, INVELOX with multiple wind turbine generator systems, *Energy* 93 (2015) 1030–1040, <https://doi.org/10.1016/j.energy.2015.09.076>.
- [10] R. Bontempo, M. Manna, Effects of the duct thrust on the performance of ducted wind turbines, *Energy* 99 (2016) 274–287, <https://doi.org/10.1016/j.energy.2016.01.025>.
- [11] B.K. Debnath, R. Das, Prediction of Performance Coefficients of a Three-Bucket Savonius Rotor Using Artificial Neural Network, 2010, pp. 1–11, <https://doi.org/10.1063/1.3467510>.
- [12] A. İlhan, S. Tümse, M.O. Tasci, M. Bilgili, B. Şahin, Particle Image Velocimetry Investigation of the Flow for the Curved Type Wind Turbine Shroud 15 (2) (2022) 373–385.
- [13] A. İlhan, H. Zontul, S. Tümse, M. Bilgili, B. Şahin, Environmental Effects Flow analyses of diffuser augmented wind turbines (2021), <https://doi.org/10.1080/15567036.2020.1861130>.
- [14] T.A. Khamlaj, M.P. Rumpfkeil, Analysis and optimization of ducted wind turbines, *Energy* (2018), <https://doi.org/10.1016/j.energy.2018.08.106>.
- [15] D. Li, C. Li, W. Zhang, H. Zhu, Effect of building diffusers on aerodynamic performance for building augmented vertical axis wind turbine, *J. Renew. Sustain. Energy* 13 (2) (2021), <https://doi.org/10.1063/5.0025742>.
- [16] N. Bekele, W. Bogale, Parametric study of a diffuser for horizontal axis wind turbine power augmentation, *AIMS Energy* 7 (6) (2019) 841–856, <https://doi.org/10.3934/energy.2019.6.841>.
- [17] A. Agha, H. Chaudhry, F. Wang, Diffuser augmented wind turbine (DAWT) technologies: a review, September (2018), <https://doi.org/10.1016/j.jweia.2007.03.004>.
- [18] S. Ahmad, W. Rafat Al, A. M El Haj, K. Khalil, S. Muath Na Bani, Analysis of accelerating devices for enclosure wind turbines, *Int. J. Astronaut. Aeronaut. Eng.* 2 (2) (2017), <https://doi.org/10.35840/2631-5009/7509>.
- [19] S. Roy, R. Das, U.K. Saha, An inverse method for optimization of geometric parameters of a Savonius- style wind turbine, *Energy Convers. Manag.* 155 (October 2017) (2018) 116–127, <https://doi.org/10.1016/j.enconman.2017.10.088>.
- [20] E. Analysis, et al., "Experimentalsimulation Performance, F O R of, Enhancement Savonius, Elliptical Turbine," 2019. November.
- [21] H. Parsa, N. Maftouni, Optimization of a real scale shrouded wind turbine using 3D CFD analysis, *Int. J. Renew. Energy Res.* 10 (2) (2020) 922–932.
- [22] A.M. El-Zahaby, A.E. Kabeel, S.S. Elsayed, M.F. Obiaa, CFD analysis of flow fields for shrouded wind turbine's diffuser model with different flange angles, *Alexandria Eng. J.* 56 (1) (2017) 171–179, <https://doi.org/10.1016/j.aej.2016.08.036>.
- [23] A.M. Elsayed, Design Optimization of Diffuser Augmented Wind Turbine, 2021, <https://doi.org/10.37934/cfdl.13.8.4559>. August.
- [24] M.A.R. Yass, E. Hussein, A. Hussein, Experimental study to design and manufacturing of NACA 0012 horizontal Axis wind turbine blade, *J. Univ. Babylon Eng. Sci.* 26 (2018) 2018.

- [25] A.P. Schaffarczyk, Introduction to wind turbine technology, *Green Energy Technol* 38 (2011) 1–29, https://doi.org/10.1007/978-1-84996-175-2_1.
- [26] Y. Ohya, T. Karasudani, A shrouded wind turbine generating high output power with wind-lens technology, *Energies* 3 (4) (2010) 634–649, <https://doi.org/10.3390/en3040634>.
- [27] B. Kosasih, A. Tondelli, Experimental study of shrouded micro-wind turbine, *Procedia Eng.* 49 (December) (2012) 92–98, <https://doi.org/10.1016/j.proeng.2012.10.116>.
- [28] B.A. Soomro, A. Ahmed, A. Hussain, S. Zulfikar, A. Bhutto, B. Ahmed, Modelling and Simulation of Diffuser Augmented Wind Turbine (DAWT) 99. Modeling and Simulation of Diffuser Augmented Wind Turbine, 2016 [Online]. Available: <https://www.researchgate.net/publication/311654129>.
- [29] L. Dhakshinamurthy, Design and analysis of diffuser augmented wind turbine using CFD, *Int. Res. J. Eng. Technol.* 7 (APRIL) (2020) 962–968.
- [30] S.A.H. Jafari, B. Kosasih, Flow analysis of shrouded small wind turbine with a simple frustum diffuser with computational fluid dynamics simulations, *J. Wind Eng. Ind. Aerodyn.* 125 (2014) 102–110, <https://doi.org/10.1016/j.jweia.2013.12.001>.
- [31] B.A.J. Al-Quraishi, et al., CFD investigation of empty flanged diffuser augmented wind turbine, *Int. J. Integr. Eng.* 12 (3) (2020) 22–32, <https://doi.org/10.30880/ijie.2020.12.03.004>.
- [32] @cadence design System, Hexahedral-Mesh-Vs-Tetrahedral-Comparing-High-Quality-Meshing, cadence CFD, 2022. <https://resources.system-analysis.cadence.com/blog/msa2022-hexahedral-mesh-vs-tetrahedral-comparing-high-quality-meshing>.
- [33] T.D. Canonsburg, ANSYS FLUENT user 's guide, *Knowl. Creat. Diffus. Util.* 15317 (October) (2012) 724–746.
- [34] Y. A. Çengel, "Heat Transfer: Unsteady Heat Transfer." <http://heattransferkarikuse.blogspot.com/2017/06/unsteady-heat-transfer.html>.
- [35] J.H. Ferziger, M. Peric, A. Leonard, Computational methods for fluid dynamics, *Phys. Today* 50 (3) (1997) 80–84, <https://doi.org/10.1063/1.881751>.
- [36] T.R. Taha, An introduction to parallel computational fluid dynamics, *IEEE Concurr* 6 (4) (2005) 78, <https://doi.org/10.1109/mcc.1998.736434>, 78.
- [37] Y.A. Çengel, J.M. Cimbala, McGraw-hill series in mechanical engineering, *Fluid Mech. Fundam. Appl.* (2006) 968.
- [38] Y. Mustafa, A comparative CFD analysis of NACA0012 and NACA4412 airfoils 2 (4) (2018) 145–159, <https://doi.org/10.30521/jes.454193>.
- [39] X. Chen, N. Katz, D. Peters, Washington University Open Scholarship Optimization of Wind Turbine Airfoils/Blades and Wind Farm Layouts, 2014.
- [40] D.A. Salam, A. Riadh, *Wind Energy State of the Art : Present and Future Technology*, vol. 7, 2020.
- [41] R.K.D. Lokesharun, S. Rameshkumar, B.S. Navaneeth, Design and analysis of diffuser augmented wind turbine using CFD, *Int. J. Mech. Ind. Eng.* 7 (October) (2019) 1–13.
- [42] Y. Ohya, T. Karasudani, A. Sakurai, Development of a shrouded wind turbine with a flanged diffuser 96 (2008) 524–539, <https://doi.org/10.1016/j.jweia.2008.01.006>.